ELSEVIER

Remote Sensing of Environment

# Stochastic Modeling of Radiation Regime in Discontinuous Vegetation Canopies

*Nikolay V. Shabanov,* Y. Knyazikhin,* Frêdêric Baret,† and Ranga B. Myneni**

*A stochastic radiative transfer equation for the mean field and its solution for the case of discontinuous vegetation canopies is discussed in this article. The equation set satisfies the law of energy conservation and is amenable to numerical solution by the method of successive orders of scattering approximations. Special attention is given to analytical analysis of the effect of spatial discontinuity on the radiation field. Research indicates that a complete description of the radiation field in discontinuous media is possible, using not only average values of radiation over total space, but averages over space occupied by absorbing elements is also required. A new formula for absorbtance, which extends the formula for a homogeneous case, was obtained for the general case of discontinuous media. The internal as well as the emergent radiation fields were validated using available radiative transfer models (one- and three-dimensional) and Monte Carlo model of computer-generated maize canopy. Additionally, the canopy reflectance simulation is assessed by comparisons with field data from shrublands. In all cases, the simulations compare well with both the Monte Carlo results and the field data.* ©*Elsevier Science Inc., 2000*

## NOMENCLATURE

H, total depth (height) of canopy
$\vec{\Omega}=\{\Omega_x,\Omega_y,\Omega_z\}$, unit vector of the solid angle
$\vec{\Omega}_0$, direction of direct solar radiation
$\mu(\vec{\Omega})$, cosine of polar angle of direction $\vec{\Omega}$
$\delta(\vec{\Omega}-\vec{\Omega}_0)$, Dirac delta function
$\chi(\vec{r})$, indicator function
$F^{\mathrm{dir}}(\lambda)$, extraterrestrial solar radiance at the top of the atmosphere
$F^{\mathrm{dir+dif}}(\lambda,\vec{\Omega}_0)$, extraterrestrial solar irradiance at the top of the canopy
$I(\vec{r},\vec{\Omega})$, radiance (intensity) at spatial point $\vec{r}$ and in direction $\vec{\Omega}$
$\bar{I}(z,\vec{\Omega})$, mean radiance, averaged over the horizontal plane at depth $z$
$U(z,\vec{\Omega})$, mean radiance, averaged over the vegetated portion of a horizontal plane $z$
$S_R(x_0,y_0)$, cylinder of height $H$, with vertical axis located at point $(x_0,y_0)$ and radius $R$
$T_z$, area of horizontal plane $z$, $z\in[0; H]$ covered by vegetation
$T_z(x_0,y_0)$, manifold $T_z$, shifted by vector $\{x_0,y_0\}$
$S_R\cap T_z$, common area of manifold $S_R$, $T_z$
Mes(S), measure of area $S$
$p(z)$, horizontal density of vegetation (HDV) at level $z$
$u_L(\vec{r})$, foliage area volume density (FAVD; $m^2/m^3$)
$\lambda$, wavelength
$r_D(\lambda)$, spectral hemispherical reflectance of the leaf
$t_D(\lambda)$, spectral hemispherical transmittance of the leaf
$\omega(\lambda)$, single-scattering leaf albedo
$\rho_{soil}(\lambda)$, soil hemispherical reflectance
$G(\vec{r},\vec{\Omega})$, mean projection of leaf normals in the direction $\vec{\Omega}$
$\frac{1}{\pi}\Gamma(\vec{r},\vec{\Omega})$, area scattering phase function
$\hat{\sigma}_s(\vec{\Omega}'\rightarrow\vec{\Omega})$, differential scattering cross-section
$\hat{\sigma}(\vec{\Omega})$, extinction coefficient

* Department of Geography, Boston University Boston
† INRA Bioclimatologie, Site Agroparc, 84914 Avignon Cedex 9, France

Address correspondence to Nikolay V. Shabanov, Department of Geography, Boston University, 675 Commonwealth Avenue, Boston, MA, 02215, USA. E-mail: shabanov@bu.edu

*Received 31 January 1999; revised 10 June 1999.*

REMOTE SENS. ENVIRON. 74:125–144 (2000)

655 Avenue of the Americas, New York, NY 10010

0034-4257/00/$–see front matter
PII S0034-4257(00)00128-0

HDRF, the hemispherical-directional reflectance factor
BHR, the bihemispherical reflectance

## INTRODUCTION

An accurate description of photon transport in vegetation canopies is of interest in many branches of contemporary science, such as optical remote sensing of vegetated land surfaces, land surface climatology, and plant physiology. The development of radiative transfer (RT) theory in vegetation canopies shows a gradual evaluation from the description of simple homogeneous media to complex discrete media. When the height of a canopy is small and the vegetation is evenly distributed on the ground (as it is in the case of crops and grasses), the turbid medium approach of a vegetated canopy is valid, and the standard 1-D RT equation (RTE) is used (Ross, 1975). In this case, the canopy is treated as a homogeneous gas with nondimensional planar scattering centers, which are not spatially correlated with one another. However, the more complex case typically occurs in nature, when individual vegetation units can be distinguished (individual trees in a forest, for example) and the effect of clustering of vegetation elements becomes important. The effect of clustering of vegetation, or the phenomenon that positions of vegetation elements tend to be correlated, exists simply because leaves arise on stems, branches, and twigs. The extreme example of lateral heterogeneity is shrubland, which is characterized by low (0.2) to intermediate (0.6) vegetation ground cover (Myneni et al., 1997). The structure of a vegetation canopy affects the signature of the radiation field reflected from the vegetation canopy (as measured by satellite sensors, for example), and the retrieval of biophysical variables from remote observations requires a precise understanding of the signal-generating mechanism. The turbid medium approximation results in poor simulations in cases where horizontal heterogeneity is pronounced, and more precise modeling is required.

The notion of gaps (or voids) between canopy clusters must be introduced along with precise description of topology of the boundary of vegetation to describe the signature of the radiation field in a discontinuous canopy. Nilson (1991) and Li and Strahler (1992) introduced a geometrical-optical approach to calculate the reflected radiance from such vegetation boundaries. They use the notion of mutual shadowing (the vegetation unit casts shadows on such units) and Bidirectional Gap Probability (the probability to see radiation reflected by the vegetation along the direction $\vec{\Omega}$ if it was illuminated by solar radiation along $\vec{\Omega}_0$) to describe the boundary of the vegetation. This approach allows an explanation for the hotspot effect (the peak in reflected radiance distribution in the retro-illumination direction, due to the absence of shadows in this direction). The approach is valid in the visible part of the solar spectrum, where one can restrict the study of radiation interaction to that scattered once from the boundary only. But in the near-infrared (NIR) region, leaf absorption is weak and scattering dominates, and the approach of Nilson and Li and Strahler is not accurate. The problem lies in an accurate description of multiple scattering and propagation of radiation into deeper parts of the canopy. Currently only the Monte Carlo method (Marshak and Ross, 1991) and other computer graphics rendering methods, such as ray tracing and radiosity methods (Borel et al., 1991) work well at all wavelengths, but they have several disadvantages, including computational expense, difficulty of adaption to user's specific needs, and lack of analytical analysis.

Another analytical approach describing leaf clumping in vegetation canopies is the statistical approach. Of importance is the problem of deriving analytical expressions or equations for moments, which characterize the stochastic radiative field in a vegetation canopy. The most critical is the expression for the first moment of the radiation field, the mean intensity. The problem of a stochastic equation for the mean field has been a highly active research field in recent years (Pomraning and Su, 1995). The first significant attempt to apply a statistical approach to describe a vegetation canopy was made by Menzhulin and Anisimov (1991). The more manageable closed system of statistical equations for mean intensity was derived initially in applications to a medium of broken clouds by Vainikko (1973a, 1973b) and later by Titov (1990) and Zuev and Titov (1996). This approach can be applied to vegetation canopies with some modifications.

In this paper, an exact stochastic radiative transfer equation for the mean intensity in a discontinuous vegetation canopy is derived. This equation is based on the work of Vainikko (1973a) for broken clouds with classical parameters of a vegetation canopy originally introduced by Ross (1975). We obtained a system of integral equations, which were solved numerically. The simulated radiation regime in a discontinuous canopy was validated in several ways, including comparison with field data from Jornada PROVE (Privette et al., 1999).

This paper is organized as follows. We review the basic concepts of radiative transfer in vegetation media and introduce the classical stochastic 3-D radiative transfer equation with the corresponding boundary conditions. The derivation of the transfer equation for the mean field using a statistical approach is described. Issues resulting from the effect of discontinuity in vegetated media and analytical description of this discontinuity (in particular, a new formula for absorptance) are discussed. Then, a numerical method for solving the transfer equation for the mean field is outlined, and issues related to speed of convergence are presented, followed by a detailed description of important outputs of model and comparisons with output from similar RTE models, with a radiation field in a Maize canopy simu-

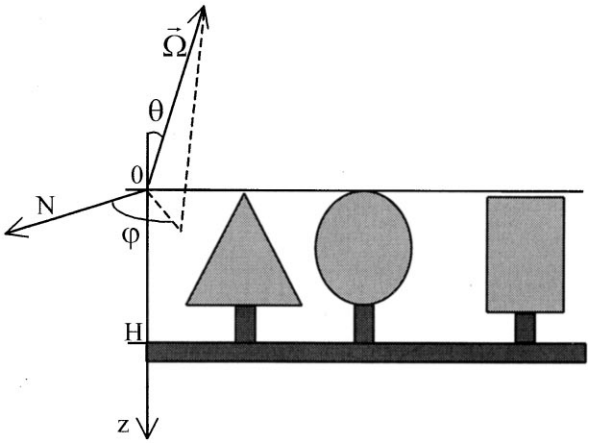


*Figure 1.* The coordinate system with vertical axis $z$ directed down. $H$ is a height of canopy; N is direction to north; $\vec{\Omega}(\theta,\varphi)$ is direction, with $\theta$ as zenith angle and $\varphi$ as azimuth angle.

lated using the Monte Carlo method and with field data from Jornada PROVE. In addition, a numerical study of the effect of discontinuity on the radiation field in a vegetation canopy is presented.

## CLASSICAL 3-D RADIATIVE TRANSFER IN VEGETATION CANOPIES

Consider a canopy of depth $H$ in a coordinate system with vertical axis $z$ directed downward (shown on Fig. 1). We describe the canopy structure with the indicator function, as shown in Eq. (1):

$$\chi(\vec{r})=\begin{cases}1, \text{ if } \vec{r}\in\text{vegetation}\\ 0, \text{ otherwise}\end{cases} \tag{1}$$

$\vec{r}$ is the coordinate triplet $[\vec{r}\sim(x,y,z)]$ with its origin at the top of the canopy. The indicator function is treated as a random variable. Its distribution function, in the general case, depends on both macroscale (e.g., random dimensions of the trees and their spatial distribution) and microscale (e.g., structural organization of an individual tree) properties of the vegetation canopy and includes all three of its components, absolute continuous, discrete, and singular (Knyazikhin et al., 1998a). It is supposed that photons interact with phytoelements only; that is, we ignore atmospheric scattering inside the later $z\in[0,H]$.

To approximate the canopy structure, a fine spatial mesh is introduced by dividing the layer $[0,H]$ into nonoverlapping fine cells $e(\vec{r})$ of size $\Delta x=\Delta y=\Delta z\equiv\varepsilon$. Each realization $\chi(\vec{r})$ of canopy structure is replaced by its mean over fine cell $e(\vec{r})$, the foliage area volume density (FAVD), as seen in Eq. (2).

$$u_L(\vec{r})=\frac{1}{\text{Mes}[e(\vec{r})]}\int\limits_{e(\vec{r})}\chi(\vec{r})d\vec{r}=\frac{1}{V}\sum_{j=1}^{N}S_j \tag{2}$$

where Mes(…) means the measure of the cell $e(\vec{r})$ (in most cases it is simply a volume), $V$ is a volume of $e(\vec{r})$, and $S_j$ is a one-sided leaf area. This integration ("smoothing") technique provides the convergence process (Knyazikhin et al., 1998a) $u_L(r)\to\chi(\vec{r})$ when $\varepsilon\to 0$, and so Eq. (2) can be taken as an approximation of the structure of the vegetation canopy. The accuracy of this approximation depends on size $\varepsilon$ of the fine cell $e(\vec{r})$. To our knowledge, all existing canopy radiation models are based on appoximations of Eq. (2) by piecewise continuous functions (e.g., describing both the spatial distribution of various geometrical objects like cones, ellipsoids, etc., and the variation of leaf area within a geometrical figure; Ross, 1975; Li and Strahler, 1992; Li at al., 1995; Nilson, 1977). Also, we assume that the density of the phytoelements in the foliated cells is constant, that is [see Eq. (3)]

$$u_L(\vec{r})=d_L\chi(\vec{r}) \tag{3}$$

where $d_L$ is the one-sided leaf area per unit volume (in $m^2/m^3$).

The vertical heterogeneity of vegetation canopy is described by a variation of horizontal density of vegetation with height, referred to later as HDV (in other words, the probability of finding foliage elements at depth $z$) and defined as seen in Eq. (4):

$$p(z)=\frac{1}{S}\int\!\!\int_{x,y}\chi(\vec{r})dxdy \tag{4}$$

Here $S$ means sufficiently large area over the horizontal plane $z$. In terms of these notations, the leaf area index (LAI) can be expressed as [see Eq. (5)]

$$\begin{aligned}\text{LAI}&=\frac{1}{S}\int_V u_L(\vec{r})dV=\frac{d_L}{S}\int_V\chi(\vec{r})dV\\ &=d_L\int_0^H d\xi\frac{1}{S}\int\!\!\int_{x,y}\chi(\vec{r})dxdy=d_L\int_0^H p(\xi)d\xi\end{aligned} \tag{5}$$

To described the interaction of canopy elements (leaves) with radiation, we use the mean projection of leaf normals in direction $\vec{\Omega}$ (Ross, 1975), as shown in Eq. (6)

$$G(\vec{r},\vec{\Omega})=\frac{1}{2\pi}\int_{2\pi^+}g_L(\vec{r},\vec{\Omega}_L)|\vec{\Omega}\cdot\vec{\Omega}_L|d\vec{\Omega}_L \tag{6}$$

and the area-scattering phase function [see Eq. (7)]

$$\frac{1}{\pi}\Gamma(\vec{r},\vec{\Omega}'\to\vec{\Omega})=\frac{1}{2\pi}\int_{2\pi^+}g_L(\vec{r},\vec{\Omega}_L)|\vec{\Omega}'\cdot\vec{\Omega}_L|\gamma_{L,\lambda}(\vec{r},\vec{\Omega}_L,\vec{\Omega}'\to\vec{\Omega})d\vec{\Omega}_L \tag{7}$$

Here $g_L(\vec{r},\vec{\Omega}_L)$ is the probability density of leaf normal orientation over the upper hemisphere and [see Eq. (8)]

$$\frac{1}{2\pi}\int_{2\pi^+}g_L(\vec{r},\vec{\Omega}_L)d\vec{\Omega}_L=1 \tag{8}$$

Optical properties of the canopy elements are described by the leaf-scattering phase function, $\gamma_{L\lambda}$ (Shultis and Myneni, 1988), as seen in Eq. (9):

$$\gamma_{L,\lambda}(\vec{r},\vec{\Omega}_L,\vec{\Omega}\rightarrow\vec{\Omega}')=\begin{cases}\frac{1}{\pi}r_D(\lambda)\cdot|\vec{\Omega}\cdot\vec{\Omega}_L|, & (\vec{\Omega}\cdot\vec{\Omega}_L)(\vec{\Omega}'\cdot\vec{\Omega}_L)<0\\ \frac{1}{\pi}t_D(\lambda)\cdot|\vec{\Omega}\cdot\vec{\Omega}_L|, & (\vec{\Omega}\cdot\vec{\Omega}_L)(\vec{\Omega}'\cdot\vec{\Omega}_L)<0\end{cases} \quad (9)$$

Here $r_D(\lambda)$ and $t_D(\lambda)$ are the spectral hemispherical reflectance and transmittance, respectively, of the leaf element. The leaf scattering phase function integrated over all exit photon directions yields the single-scattering leaf albedo (per unit leaf area), $\omega(\lambda)$, that is [see Eq. (10)]

$$\int_{4\pi}\gamma_{L,\lambda}(\vec{r},\vec{\Omega}_L,\vec{\Omega}\rightarrow\vec{\Omega}')d\vec{\Omega}'=\omega(\lambda) \quad (10)$$

With this background information, we can compactly represent the extinction coefficient $\sigma(\vec{\Omega})$ and the differential scattering coefficient $\sigma_s(\vec{\Omega}'\rightarrow\vec{\Omega})$ (Ross, 1975) as seen in Eq. (11)

$$u_L(\vec{r})G(\vec{r},\vec{\Omega})=d_L\chi(\vec{r})G(\vec{r},\vec{\Omega})=\sigma(\vec{\Omega})\chi(\vec{r})=\hat{\sigma}(\vec{r},\vec{\Omega}) \quad (11)$$

and Eq. (12)

$$\frac{u_L(\vec{r})}{\pi}\Gamma(\vec{r},\vec{\Omega}'\rightarrow\vec{\Omega})=\frac{d_L\chi(\vec{r})}{\pi}\Gamma(\vec{r},\vec{\Omega}'\rightarrow\vec{\Omega})$$
$$=\sigma_s(\vec{\Omega}'\rightarrow\vec{\Omega})\chi(\vec{r})=\hat{\sigma}_s(\vec{r},\vec{\Omega}'\rightarrow\vec{\Omega}) \quad (12)$$

The radiation regime in such a canopy is described by the transport equation, shown in Eq. (13)

$$\vec{\Omega}\cdot\nabla I(\vec{r},\vec{\Omega})+\chi(\vec{r})\sigma(\vec{\Omega})I(\vec{r},\vec{\Omega})$$
$$=\chi(\vec{r})\int_{4\pi}\sigma_s(\vec{\Omega}'\rightarrow\vec{\Omega})I(\vec{r},\vec{\Omega}')d\vec{\Omega}' \quad (13)$$

This equation will be referred to later as the "classical stochastic radiative transfer equation." It differs from nonstochastic [introduced for turbid media by Ross (1975)] by the indicator function $\chi(\vec{r})$, which modifies the second and third term of Eq. (13).

An important feature of the radiation regime in vegetation canopies is the hot-spot effect, which is the peak in reflected radiance distribution along the retro-illumination direction. The standard theory describes the hot-spot by modifying the extinction coefficient $\sigma(\Omega)$, namely (Marshak, 1989) [see Eq. (14)]

$$\sigma(\vec{\Omega},\vec{\Omega}_0)=\sigma(\vec{\Omega})\cdot h(\vec{\Omega},\vec{\Omega}_0), \quad (14)$$

where $h(\vec{\Omega},\vec{\Omega}_0)$ is [see Eq. (15)]

$$h(\vec{\Omega},\vec{\Omega}_0)$$
$$=\begin{cases}1-\sqrt{\frac{G(\vec{\Omega}_0)|\mu(\vec{\Omega})|}{G(\vec{\Omega})|\mu(\vec{\Omega}_0)|}}\exp[-\Delta(\vec{\Omega},\vec{\Omega}_0)\cdot k], & \text{if}(\vec{\Omega}\cdot\vec{\Omega}_0)<0\\ 1, & \text{if } (\vec{\Omega}\cdot\vec{\Omega}_0)>0\end{cases} \quad (15)$$

and [see Eq. (16)]

$$\Delta(\vec{\Omega},\vec{\Omega}_0)=\sqrt{\frac{1}{\mu^2(\vec{\Omega}_0)}+\frac{1}{\mu^2(\vec{\Omega})}+\frac{2(\vec{\Omega}_0\cdot\vec{\Omega})}{|\mu(\vec{\Omega})\mu(\vec{\Omega}_0)|}} \quad (16)$$

In the equation above, $\mu(\vec{\Omega})$ denotes the cosine of the polar angle of direction $\vec{\Omega}$ and $k$ is an empirical parameter, related to the ratio of vegetation height to characteristic leaf dimension. Its value was estimated to be between 1 and 8 based on several sets of experimental data (Stewart, 1990).

To find a unique solution of Eq. (13), it is necessary to specify the radiance penetrating into the canopy through upper ($z$=0) and lower ($z$=H) boundaries. The canopy is illuminated from above by both direct monodirectional solar component in direction $\vec{\Omega}_0$, $[\mu_0(\vec{\Omega}_0)<0]$, namely $F^{\text{dir}}(\lambda)\delta(\Omega-\Omega_0)$, as well as by diffuse radiation from the sky, $\tilde{d}(\vec{\Omega},\vec{\Omega}_0)$. At the ground, the corresponding boundary condition is the radiation reflected from the ground, as seen on Eq. (17)

$$\begin{cases}I(0,\vec{\Omega})=F^{\text{dir}}(\lambda)\delta(\vec{\Omega}-\vec{\Omega}_0)+\tilde{d}(\vec{\Omega},\vec{\Omega}_0), & \mu(\vec{\Omega})<0\\ I(H,\vec{\Omega})=I_H(\vec{\Omega}), & \mu(\vec{\Omega})>0\end{cases} \quad (17)$$

The canopy bottom is assumed to be a horizontally homogeneous Lambertian surface. in this case the function $I_H(\vec{\Omega})$ can be expressed as shown in Eq. (18):

$$I_H(\vec{\Omega})=\frac{\rho_{\text{soil}}(\lambda)}{\pi}\int_{2\pi}I(H,\vec{\Omega})|\mu(\vec{\Omega})|d\vec{\Omega} \quad (18)$$

where $\rho_{soil}(\lambda)$ is the soil hemispherical reflectance.

The incoming radiation can be parameterized in terms of two scalar values: $F^{\text{dir+dif}}(\lambda,\vec{\Omega}_0)$, total flux defined as [see Eq. (19)]

$$F^{\text{dir+dif}}(\lambda,\vec{\Omega}_0)\equiv\int_{2\pi-}I(0,\vec{\Omega})|\mu(\vec{\Omega})|d\vec{\Omega}$$
$$=\int_{2\pi-}[F^{\text{dir}}(\lambda)\delta(\vec{\Omega}-\vec{\Omega}_0)+\tilde{d}(\vec{\Omega},\vec{\Omega}_0)]|\mu(\vec{\Omega})|\text{d}\vec{\Omega}$$
$$=F^{\text{dir}}(\lambda)|\mu(\vec{\Omega}_0)|+\int_{2\pi-}\tilde{d}(\vec{\Omega},\vec{\Omega}_0)|\mu(\vec{\Omega})|d\vec{\Omega} \quad (19)$$

and $f_{\text{dir}}(\lambda,\vec{\Omega}_0)$ is the ratio of direct radiation incident on the top of plant canopy to the total incident irradiance [see Eq. (20)]

$$f_{\text{dir}}(\lambda,\vec{\Omega}_0)\equiv\frac{F^{\text{dir}}(\lambda)|\mu(\vec{\Omega}_0)|}{F^{\text{dir+dif}}(\lambda,\vec{\Omega}_0)}\in[0;1] \quad (20)$$

Equations (19) and (20) explain the following formula for incoming solar radiation [see Eq. (21)]

$$F^{\text{dir}}(\lambda)\delta(\vec{\Omega}-\vec{\Omega}_0)+\tilde{d}(\vec{\Omega},\vec{\Omega}_0)\equiv F^{\text{dir+dir}}(\lambda,\vec{\Omega}_0)$$
$$\times\left\{\frac{f_{\text{dir}}(\lambda,\vec{\Omega}_0)}{|\mu(\vec{\Omega}_0)|}\delta(\vec{\Omega}-\vec{\Omega}_0)+[1-f_{\text{dir}}(\lambda,\vec{\Omega}_0)]d(\vec{\Omega},\vec{\Omega}_0)\right\} \quad (21)$$

The general boundary value problem [Eqs. (13) and (17)] can be split into two simpler subproblems: (1) black soil (BS) problem, where the soil is assumed to be 100% absorbing. For this problem we set additionally the upper boundary condition ($z$=0) to be the same as in Eq. (17), so the problem is defined by Eq. (13) and the boundary condition [see Eq. (22)]

$$\begin{cases}I(0,\vec{\Omega})=F^{\text{dir+dif}}(\lambda,\vec{\Omega}_0)\left\{\frac{f_{\text{dif}}(\lambda,\vec{\Omega}_0)}{|\mu(\vec{\Omega}_0)|}\delta(\vec{\Omega}-\vec{\Omega}_0)\right.\\ \qquad\left.+[1-f_{\text{dir}}(\lambda,\vec{\Omega}_0)]d(\vec{\Omega},\vec{\Omega}_0)\right\}, \quad \mu(\vec{\Omega})<0\\ I(H,\vec{\Omega})=0, \quad \mu(\vec{\Omega})>0\end{cases} \quad (22)$$

The solution of BS problem is referred to later as $I_\lambda^{BS}(r,\vec{\Omega})$; $I_\lambda^{BS}(r,\vec{\Omega})$ depends on sun-view geometry, canopy architecture, and spectral properties of the leaves; (2) soil (S) problem. In this case there is no input of energy from above, but the source intensity $I(H,\vec{\Omega})$ is located at the bottom of the canopy. In the case of Lambertian surface $I(H,\vec{\Omega})=1/\pi$, the S problem is defined by Eq. (13) and the boundary condition [see Eq. (23)]

$$\begin{cases} I(0,\vec{\Omega})=0, & \mu(\vec{\Omega})<0 \\ I(H,\vec{\Omega})=\dfrac{1}{\pi}, & \mu(\vec{\Omega})>0 \end{cases} \tag{23}$$

Similarly, the solution of S problem is referred to later as $I_\lambda^{S}(r,\vec{\Omega})$; $I_\lambda^{S}(r,\vec{\Omega})$ depends on the spectral properties of the leaves and canopy structure only.

The reasons for splitting the problem are as follows. First, we separate the influence of soil; that is, the solution of the general case is constructed from soil-independent S/BS solutions and effective soil reflectance. This can save computational effort, if we need to solve the RTE for different soil patterns keeping other parameters constant. Second, we substitute a complex boundary condition on the soil boundary in the general case (integral from unknown solution) to simple functions known in advance at boundaries for both subproblems. Our numerical procedure to solve mean RTE significantly uses this fact [see Eq. (24)]

$$I_\lambda(r,\vec{\Omega}) \approx \left\{ I_\lambda^{BS}(r,\vec{\Omega}) + \frac{\rho_{soil}(\lambda)}{1-\rho_{soil}(\lambda)\cdot R_S(\lambda)} \cdot T_{BS}(\lambda)\cdot I_\lambda^{S}(r,\vec{\Omega}) \right\} \cdot F^{dir+dif}(\lambda,\vec{\Omega}_0) \tag{24}$$

for reflectance (albedo) [see Eq. (25)]

$$R(\lambda)\approx R_{BS}(\lambda)+\frac{\rho_{soil}(\lambda)}{1-\rho_{soil}(\lambda)\cdot R_S(\lambda)}\cdot T_{BS}(\lambda)\cdot T_S(\lambda) \tag{25}$$

for absorbtance [see Eq. (26)]

$$A(\lambda)\approx A_{BS}(\lambda)+\frac{\rho_{soil}(\lambda)}{1-\rho_{soil}(\lambda)\cdot R_S(\lambda)}\cdot T_{BS}(\lambda)\cdot A_S(\lambda) \tag{26}$$

and transmittance [see Eq. (27)]

$$T(\lambda)\approx T_{BS}(\lambda)+\frac{\rho_{soil}(\lambda)}{1-\rho_{soil}(\lambda)\cdot R_S(\lambda)}\cdot T_{BS}(\lambda)\cdot R_S(\lambda) \tag{27}$$

where $R_i(\lambda)$, $T_i(\lambda)$, $A_i(\lambda)$ are the hemispherical reflectance, transmittance, and absorbtance for corresponding $i$ problem ($i$=S or BS problem). Note that we can replace the approximate equality in the formulas above by exact equality only for the horizontally homogeneous special case of mean RTE [mathematically, it means $K(z,\xi\vec{\Omega})\equiv p(\xi)$]. In any other cases formulas are only approximately valid (Knyazikhin et al., 1998b).

It must be noted that in the case of discontinuous vegetation canopy, the influence of soil can be quite high due to the presence of gaps in the vegetation. So it is useful to consider the case of non-Lambertian anisotropic soil. In this case, using BS/S split of the general problem, we should make the following changes to the formulas shown above (Knyazikhin et al., 1998c): BS problem, no changes; S problem; change boundary condition $I(H,\vec{\Omega})$ as follows [see Eq. (28)]

$$I(H,\vec{\Omega})=\frac{R(\vec{\Omega},\vec{\Omega}_0)}{\pi\int\limits_{2\pi+} R(\vec{\Omega},\vec{\Omega}_0)|\mu(\vec{\Omega})|d\vec{\Omega}} \tag{28}$$

here, $R(\vec{\Omega},\vec{\Omega}_0)$, is bidirectional soil reflectance factor; in Eqs. (24) through (27) it is necessary to introduce effective soil reflectance instead of $\rho(\lambda)$ as shown in Eq. (29)

$$\rho_{eff}(\lambda)=\frac{1}{\pi}\int\limits_{2\pi+} R(\vec{\Omega},\vec{\Omega}_0)|\mu(\vec{\Omega})|d\vec{\Omega} \tag{29}$$

## TRANSFER EQUATION FOR THE MEAN INTENSITY

The motivation to find mean intensity of solar radiation interacting with vegetation canopy is simple: sensors aboard satellite platforms measure the mean field emanating from the smallest area to be resolved, from a pixel. One possible modeling approach to this problem is to generate the set of stochastic realizations of vegetation canopies, solve the classical stochastic RTE [Eq. (13)], and average the solutions. A highly desirable alternative to this computationally demanding process is to derive a transport equation for the mean field directly. As was mentioned, the closed system of equations describing mean intensity of radiation was developed for broken clouds by Vainikko (1973a, 1973b), and it can be applied to vegetation canopies.

In this section, we will use Vainikko's approach to develop the equations describing the mean intensity of radiation in the vegetation canopy. We will be interested in two kinds of mean intensities in vegetation canopies, defined as follows: (1) the mean intensity over a vegetated area, at the level $z\in[0,H]$ [see Eq. (30)]

$$U(z,\vec{\Omega})=\lim_{R\to\infty}\frac{1}{\mathrm{Mes}(S_R\cap T_z)}\iint\limits_{S_R\cap T_z} I(x,y,z,\vec{\Omega})dxdy \tag{30}$$

where $T_z$ is part of a horizontal plane $z$ covered by vegetation, and $\mathrm{Mes}(S_R\cap T_z)$ denotes the area of plane $z$ covered by vegetation that is inside of a bounding circle $S_R$, defined at the same plane; and (2) the mean intensity over the total space at the level $z\in[0,H]$ [see Eq. (31)]

$$\bar{I}(z,\vec{\Omega})=\lim_{R\to\infty}\frac{1}{\pi R^2}\iint\limits_{S_R} I(x,y,z,\vec{\Omega})dxdy \tag{31}$$

We assume that the following important property of stochastic intensity $I(\vec{r},\vec{\Omega})$ is valid [see Eq. (32)]

$$U(z,\vec{\Omega})=\lim_{R\to\infty}\frac{1}{\mathrm{Mes}[S_R\cap T_z\cap T_\xi(x_1,y_1)]} \times \iint\limits_{S_R\cap T_z\cap T_\xi(x_1,y_1)} I(x,y,z,\vec{\Omega})dxdy \tag{32}$$

which simply means that manifold $T_z \cap T_\xi(x_1,y_1)$ contains the same percentage of vegetation as the total manifold $T_z$). This is the so-called assumption of "local chaotisity and global order" (Vainikko, 1973a).

The procedure to derive the transfer equation for mean intensity from the classical approach is the following: First, the classical stochastic transfer equation is integrated from boundaries [$z=0$ and $z=H$) to some inner point $z \in [0,H]$ to obtain a linear integral equation, which still describes a particular random realization of vegetated elements. Second, the transfer equation is averaged over the whole plane $z$ to derive a formula for $\bar{I}(z,\vec{\Omega})$, which is the mean intensity over the whole horizontal plane. The equation for $\bar{I}(z,\vec{\Omega})$ depends on $U(z,\vec{\Omega})$, as seen in Eq. (33)

$$\bar{I}(z,\vec{\Omega})=f[U(z,\vec{\Omega}), \ldots] \tag{33}$$

Third, the transfer equation is averaged over part of a horizontal plane $z$, which is covered by vegetation [$\chi(\vec{r})=1$], to derive the system for unknown $U(z,\vec{\Omega})$, which is the mean radiance over the vegetated portion of plane.

The averaging procedure, as a general rule, results in equations that contain some parameters descriptive of characteristic moments for the media (correlation function and mean value). The equations for $\bar{I}(z,\vec{\Omega})$ and $U(z,\vec{\Omega})$ depend on the following mean statistical functions, which must be obtained through corresponding procedure of modeling the vegetation [see Eq. (34)]

$$q(z,\xi,\vec{\Omega})=\lim_{R\to\infty}\frac{\mathrm{Mes}\left\{S_R\cap T_z\cap T_\xi\left[\frac{\Omega_x}{\Omega_z}(z-\xi),\frac{\Omega_y}{\Omega_z}(z-\xi)\right]\right\}}{\pi R^2} \tag{34}$$

which is the probability of finding simultaneously the vegetation elements at locations $M_1(x,y,z)$ and $M_2(\mu,\eta,\xi)$ along the direction $\vec{\Omega}$. In the above [see Eq. (35)]

$$\mathrm{Mes}\left\{S_R\cap T_z\cap T_\xi\left[\frac{\Omega_x}{\Omega_z}(z-\xi),\frac{\Omega_y}{\Omega_z}(z-\xi)\right]\right\} \tag{35}$$

shows the part of vegetation located on a horizontal plane at depth $z$ that will overlap with vegetation located on a horizontal plane at depth $\xi$, if the two planes are moved toward one another along $\vec{\Omega}$ while keeping them parallel until they collapse. Further [see Eq. (36)]

$$p(z)=\lim_{R\to\infty}\frac{\mathrm{Mes}\{S_R\cap T_z\}}{\pi R^2} \tag{36}$$

is the probability of finding foliage elements at depth $z$, or HDV [as defined earlier at Eq. (4)]. And [see Eq. (37)]

$$K(z,\xi,\vec{\Omega})=\frac{q(z,\xi,\vec{\Omega})}{p(z)} \tag{37}$$

is the conditional probability of finding a vegetation element at point $M_2(\mu,\eta,\xi)$, which is located along the direction $\vec{\Omega}$ from $M_1(x,y,z)$ in the plane $\xi$ given $M_1(x,y,z)$ belongs vegetation.

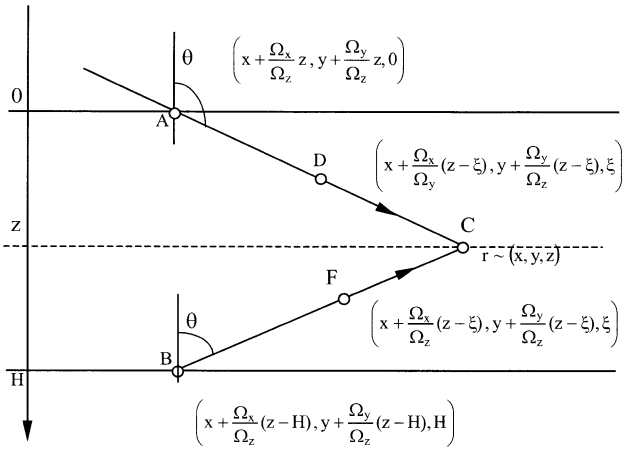


*Figure 2.* Procedure for integration of RTE. Points A and B correspond to the starting points of integration (located on boundaries), which is performed along the direction $\theta$ up to the inner point C, which has the coordinates $(x,y,z)$. Points D and F designate any point located on lines AC and BC. The 3-D equation of lines AC and BC is given (the parameter, controlling location on the line is $\xi$).

The detailed procedure to derive the mean RTE is as follows [we follow the procedure of Vainikko (1973a)]. We start with Eq. (13) and rewrite it in the form shown in Eq. (38).

$$\Omega_x\frac{\partial I(x,y,z,\vec{\Omega})}{\partial x}+\Omega_y\frac{\partial I(x,y,z,\vec{\Omega})}{\partial y}+\Omega_z\frac{\partial I(x,y,z,\vec{\Omega})}{\partial z}=g(x,y,z,\vec{\Omega}) \tag{38}$$

where [see Eq. (39)]

$$g(x,y,z,\vec{\Omega})\equiv-\chi(\vec{r})\sigma(\vec{\Omega})I(\vec{r},\vec{\Omega})+\chi(\vec{r})\int_{4\pi}\sigma_S(\vec{\Omega}'\to\vec{\Omega})I(\vec{r},\vec{\Omega})d\vec{\Omega}' \tag{39}$$

Integration of Eq. (38) from boundaries ($z=0$ and $z=H$) to some inner point $\vec{r}\sim(x,y,z)$, $z\in[0,H]$ along the direction $\vec{\Omega}$ (Fig. 2) results in the system of equations shown in Eq. (40)

$$\begin{cases} I(x,y,z,\vec{\Omega})=I(x,y,0,\vec{\Omega})+\dfrac{1}{|\mu(\vec{\Omega})|} \\ \qquad\qquad \times\displaystyle\int_0^z g\left\{x+\frac{\Omega_z}{\Omega_z}(z-\xi),y+\frac{\Omega_y}{\Omega_z}(z-\xi),\xi,\Omega\right\}d\xi, \quad \mu(\vec{\Omega})<0 \\ I(x,y,z,\vec{\Omega})=I(x,y,H,\vec{\Omega})+\dfrac{1}{|\mu(\vec{\Omega})|} \\ \qquad\qquad \times\displaystyle\int_z^H g\left\{x+\frac{\Omega_x}{\Omega_z}(z-\xi),y+\frac{\Omega_y}{\Omega_z}(z-\xi)\xi,\Omega\right\}d\xi, \quad \mu(\vec{\Omega})>0 \end{cases} \tag{40}$$

Inserting formulas for the function $g(x,y,z,\vec{\Omega})$ [Eq. (39)] into Eq. (40), we obtain the following system [see Eq. (41)]:

$$\begin{cases} I(x,y,z,\vec{\Omega})+\dfrac{1}{|\mu(\vec{\Omega})|}\displaystyle\int_0^z \chi(\ldots)\sigma(\vec{\Omega})I(\ldots,\vec{\Omega})d\xi \\ \quad=\dfrac{1}{|\mu(\vec{\Omega})|}\displaystyle\int_0^z d\xi\chi(\ldots)\int_{4\pi}\sigma_s(\vec{\Omega}'\to\vec{\Omega})I(\ldots,\vec{\Omega}') \\ \quad\times d\vec{\Omega}'+I(x,y,0,\vec{\Omega}), \quad \Omega_z<0 \\ I(x,y,z,\vec{\Omega})+\dfrac{1}{|\mu(\vec{\Omega})|}\displaystyle\int_z^H \chi(\ldots)\sigma(\vec{\Omega})I(\ldots,\vec{\Omega})d\xi \\ \quad=\dfrac{1}{|\mu(\vec{\Omega})|}\displaystyle\int_z^H d\xi\chi(\ldots)\int_{4\pi}\sigma_s(\vec{\Omega}'\to\vec{\Omega})I(\ldots,\vec{\Omega}') \\ \quad\times d\vec{\Omega}'+I(x,y,H,\vec{\Omega}), \quad \Omega_z>0 \end{cases} \tag{41}$$

where for simplicity the following shortcut was introduced [see Eq. (42)]

$$\ldots\equiv x+\frac{\Omega_x}{\Omega_z}(z-\xi),y+\frac{\Omega_y}{\Omega_z}(z-\xi),\xi \tag{42}$$

The next step is to average Eq. (41) over the horizontal plane $z$, $z\in[0,H]$. The main problem is to average the term $\chi(\ldots)I(\ldots,\vec{\Omega})$. It can be done in a straightforward manner after shifting manifold $T_\xi$ by vector $\left[\frac{\Omega_x}{\Omega_z}(z-\xi), \frac{\Omega_y}{\Omega_z}(z-\xi)\right]$, namely [see Eq. (43)]

$$\begin{aligned} &\frac{1}{\pi R^2}\iint_{S_R}\chi(\ldots)I(\ldots,\vec{\Omega})dxdy \\ &\quad=\frac{1}{\pi R^2}\iint_{S_R\cap T_\xi\left[\frac{\Omega_x}{\Omega_z}(z-\xi),\frac{\Omega_y}{\Omega_z}(z-\xi)\right]}\chi(\ldots)I(\ldots,\vec{\Omega})dxdy \\ &\quad=\frac{\mathrm{Mes}(S_R'\cap T_\xi)}{\pi R^2}\frac{1}{\mathrm{Mes}(S_R'\cap T_\xi)}\iint_{S_R'\cap T_\xi}I(x',y',\xi',\vec{\Omega})dx'dy' \end{aligned} \tag{43}$$

where [see Eq. (44)]

$$S_R'=S_R\left[\frac{\Omega_x}{\Omega_z}(z-\xi),\frac{\Omega_y}{\Omega_z}(z-\xi)\right] \tag{44}$$

If we recall Eq. (36), as seen in Eq. (45)

$$p(z)=\lim_{R\to\infty}\frac{\mathrm{Mes}\{S_R\cap T_z\}}{\pi R^2} \tag{45}$$

we obtain the next limit [see Eq. (46)]

$$\lim_{R\to\infty}\frac{1}{\pi R^2}\iint_{S_R}\chi(\ldots)I(\ldots,\vec{\Omega})dxdy=p(\xi)\cdot U(\xi,\vec{\Omega}) \tag{46}$$

Keeping in mind Eq. (46) while averaging Eq. (41) over the entire plane $z$, we finally have [see Eq. (47)]

$$\begin{cases} \bar{I}(z,\vec{\Omega})+\dfrac{1}{|\mu(\vec{\Omega})|}\displaystyle\int_0^z\sigma(\vec{\Omega})p(\xi)U(\xi,\vec{\Omega})d\xi \\ \quad=\dfrac{1}{|\mu(\vec{\Omega})|}\displaystyle\int_0^z d\xi p(\xi)\int_{4\pi}\sigma_s(\vec{\Omega}'\to\vec{\Omega})U(\xi,\vec{\Omega}') \\ \quad\times d\vec{\Omega}'+I(x,y,0,\vec{\Omega}), \quad \Omega_z<0 \\ \bar{I}(z,\vec{\Omega})+\dfrac{1}{|\mu(\vec{\Omega})|}\displaystyle\int_z^H\sigma(\vec{\Omega})p(\xi)U(\xi,\vec{\Omega})d\xi \\ \quad=\dfrac{1}{|\mu(\vec{\Omega})|}\displaystyle\int_z^H d\xi p(\xi)\int_{4\pi}\sigma_s(\vec{\Omega}'\to\vec{\Omega})U(\xi,\vec{\Omega}') \\ \quad\times d\vec{\Omega}'+\bar{I}(x,y,H,\vec{\Omega}), \quad \Omega_z>0 \end{cases} \tag{47}$$

The last step is to average the system of Eq. (41) over the portion of horizontal plane $z$, $z\in[0,H]$, covered by vegetation, $T_z$. Now we need the value of $\chi(\ldots)I(\ldots,\vec{\Omega})$ after averaging over $T_z$ [see Eq. (48)]

$$\begin{aligned} &\frac{1}{\mathrm{Mes}(S_R\cap T_z)}\iint_{S_R\cap T_z}\chi(\ldots)I(\ldots,\vec{\Omega})dxdy \\ &\quad=\frac{1}{\mathrm{Mes}(S_R\cap T_z)}\iint_{S_R\cap T_z\cap T_\xi\left[\frac{\Omega_x}{\Omega_z}(z-\xi),\frac{\Omega_y}{\Omega_z}(z-\xi)\right]}\chi(\ldots)I(\ldots,\vec{\Omega})dxdy \\ &\quad=\frac{\mathrm{Mes}(S_R'\cap T_z'\cap T_\xi)/\pi R^2}{\mathrm{Mes}(S_R\cap T_z)/\pi R^2}\frac{1}{\mathrm{Mes}(S_R'\cap T_\xi)} \\ &\quad\times\iint_{S_R'\cap T_z'\cap T_\xi}I(x',y',\xi',\vec{\Omega})dx'dy' \end{aligned} \tag{48}$$

where $T_z'=T_z\left[\frac{\Omega_x}{\Omega_z}(z-\xi),\frac{\Omega_y}{\Omega_z}(z-\xi)\right]$. Taking into account [see Eq. (49)]

$$\mathrm{Mes}(S_R'\cap T_z'\cap T_\xi)=\mathrm{Mes}\left\{S_R\cap T_z\cap T_z\left[\frac{\Omega_x}{\Omega_z}(z-\xi),\frac{\Omega_y}{\Omega_z}(z-\xi)\right]\right\} \tag{49}$$

we obtain Eq. (50):

$$\lim_{R\to\infty}\frac{1}{\mathrm{Mes}(S_R\cap T_z)}\iint_{S_R}\chi(\ldots)I(\ldots,\vec{\Omega})dxdy=K(z,\xi,\vec{\Omega})U(\xi,\vec{\Omega}) \tag{50}$$

Keeping in mind Eq. (50) while averaging Eq. (41) over $T_z$, we finally have Eq. (51):

$$\begin{cases} U(z,\vec{\Omega})+\dfrac{1}{|\mu(\vec{\Omega})|}\displaystyle\int_0^z\sigma(\vec{\Omega})K(z,\xi,\vec{\Omega})U(\xi,\vec{\Omega})d\xi \\ \quad=\dfrac{1}{|\mu(\vec{\Omega})|}\displaystyle\int_0^z d\xi K(z,\xi,\vec{\Omega})\int_{4\pi}\sigma_s(\vec{\Omega}'\to\vec{\Omega})U(\xi,\vec{\Omega}') \\ \quad\times d\vec{\Omega}'+\bar{I}(x,y,0,\vec{\Omega}), \quad \Omega_z<0 \\ U(z,\vec{\Omega})+\dfrac{1}{|\mu(\vec{\Omega})|}\displaystyle\int_z^H\sigma(\vec{\Omega})K(z,\xi,\vec{\Omega})U(\xi,\vec{\Omega})d\xi \\ \quad=\dfrac{1}{|\mu(\vec{\Omega})|}\displaystyle\int_z^H d\xi K(z,\xi,\vec{\Omega})\int_{4\pi}\sigma_s(\vec{\Omega}'\to\vec{\Omega})U(\xi,\vec{\Omega}') \\ \quad\times d\vec{\Omega}'+\bar{I}(x,y,H,\vec{\Omega}), \quad \Omega_z>0 \end{cases} \tag{51}$$

The systems in Eqs. (47) and (51) together form a complete set of equations to determine mean intensity of radiation in vegetation canopy.

**Direct and Diffuse Components of $U(z,\vec{\Omega})$**

To be consistent with boundary conditions [Eq. (17)], the function $U(z,\vec{\Omega})$ can be represented as shown in Eq. (52):

$$\begin{aligned} U(z,\vec{\Omega}) &= F^{\mathrm{dir}}(\lambda)U_\delta(z)\delta(\vec{\Omega}-\vec{\Omega}_0)+F^{\mathrm{dir+dif}}(\lambda,\vec{\Omega}_0)U_d(z,\vec{\Omega}) \\ &\equiv F^{\mathrm{dir+dif}}(\lambda,\vec{\Omega}_0)\left[\frac{f_{\mathrm{dir}}(\lambda,\vec{\Omega}_0)}{|\mu(\vec{\Omega}_0)|}U_\delta(z)\delta(\vec{\Omega}-\vec{\Omega}_0)+U_d(z,\vec{\Omega})\right] \end{aligned} \tag{52}$$

where $U_\delta(z)$ is the direct component and $U_d(z,\vec{\Omega})$ is the diffuse component of total mean intensity over the vegetated area. Inserting Eq. (52) into Eq. (51) we obtain equations for these two functions. In the equation for $U_\delta(z)$, the direct component is [see Eq. (53)]

$$U_\delta(z)+\frac{\sigma(\vec{\Omega}_0)}{|\mu(\vec{\Omega}_0)|}\int_0^z K(z,\xi,\vec{\Omega}_0)U_\delta(\xi)d\xi=1 \tag{53}$$

In the system of equations for $U_d(z,\vec{\Omega})$, the diffuse components are shown Eq. (54):

$$\begin{cases} U_d(z,\vec{\Omega})+\dfrac{\sigma(\vec{\Omega})}{|\mu(\vec{\Omega})|}\displaystyle\int_0^z K(z,\xi,\vec{\Omega})U_d(\xi,\vec{\Omega})d\xi \\ \quad =\dfrac{1}{|\mu(\vec{\Omega})|}\displaystyle\int_0^z K(z,\xi,\vec{\Omega})S(\xi,\vec{\Omega})d\xi+U_0^d(z,\vec{\Omega},\vec{\Omega}_0), \quad \mu<0 \\ U_d(z,\vec{\Omega})+\dfrac{\sigma(\vec{\Omega})}{|\mu(\vec{\Omega})|}\displaystyle\int_z^H K(z,\xi,\vec{\Omega})U_d(\xi,\vec{\Omega})d\xi \\ \quad =\dfrac{1}{|\mu(\vec{\Omega})|}\displaystyle\int_z^H K(z,\xi,\vec{\Omega})S(\xi,\vec{\Omega})d\xi+U_H^d(z,\vec{\Omega},\vec{\Omega}_0), \quad \mu>0 \\ \text{where:} \\ \quad S(\xi,\vec{\Omega})=\displaystyle\int_{4\pi}\sigma_s(\vec{\Omega}'\to\vec{\Omega})U_d(\xi,\vec{\Omega}')d\vec{\Omega}', \\ U_o^d(z,\vec{\Omega},\vec{\Omega}_0)=\dfrac{f_{\mathrm{dir}}(\lambda,\vec{\Omega}_0)\sigma_s(\vec{\Omega}_0\to\vec{\Omega})}{|\mu(\vec{\Omega})\mu(\vec{\Omega}_0)|}\displaystyle\int_0^z K(z,\xi,\vec{\Omega})U_\delta(\xi)d\xi \\ \qquad +[1-f_{\mathrm{dir}}(\lambda,\vec{\Omega}_0)]d(\vec{\Omega},\vec{\Omega}_0), \quad \mu<0 \\ U_H^d(z,\vec{\Omega},\vec{\Omega}_0)=\dfrac{f_{\mathrm{dir}}(\lambda,\vec{\Omega}_0)\sigma_s(\vec{\Omega}_0\to\vec{\Omega})}{|\mu(\vec{\Omega})\mu(\vec{\Omega}_0)|} \\ \qquad \times\displaystyle\int_z^H K(z,\xi,\vec{\Omega})U_\delta(\xi)d\xi+I_H(\vec{\Omega}), \quad \mu>0 \end{cases} \tag{54}$$

**Direct and Diffuse Components of $\bar{I}(z,\vec{\Omega})$**

Similar to the case of $U(z,\vec{\Omega})$, the function $\bar{I}(z,\vec{\Omega})$ should be consistent with the boundary condition [Eq. (17)] and can be represented as shown in Eq. (55):

$$\begin{aligned} \bar{I}(z,\vec{\Omega}) &= F^{\mathrm{dir}}(\lambda)\bar{I}_\delta(z)\delta(\vec{\Omega}-\vec{\Omega}_0)+F^{\mathrm{dir+dif}}(\lambda,\vec{\Omega}_0)\bar{I}_d(z,\vec{\Omega}) \\ &\equiv F^{\mathrm{dir+dif}}(\lambda,\vec{\Omega}_0)\left[\frac{f_{\mathrm{dir}}(\lambda,\vec{\Omega}_0)}{|\mu(\vec{\Omega}_0)|}\bar{I}_\delta(z)\delta(\vec{\Omega}-\vec{\Omega}_0)+\bar{I}_d(z,\vec{\Omega})\right] \end{aligned} \tag{55}$$

where $\bar{I}_\delta(z)$ is the direct component and $\bar{I}_d(z,\vec{\Omega})$ is the diffuse component of total mean intensity over total space. Combining Eq. (47) and Eq. (55) we obtain equations for these two functions. The equation for the direct component, $\bar{I}_\delta(z)$, is shown in Eq. (56)

$$\bar{I}_\delta(z)=1-\frac{\sigma(\vec{\Omega}_0)}{|\mu(\vec{\Omega}_0)|}\int_0^z p(\xi)U_\delta(\xi)d\xi \tag{56}$$

The system of equations for $\bar{I}_d(z,\Omega)$, the diffuse component is shown in Eq. (57)

$$\begin{cases} \bar{I}_d(z,\vec{\Omega})=-\dfrac{\sigma(\vec{\Omega})}{|\mu(\vec{\Omega})|}\displaystyle\int_0^z p(\xi)U_d(\xi,\vec{\Omega})d\xi+\dfrac{1}{|\mu(\vec{\Omega})|} \\ \qquad \times\displaystyle\int_0^z p(\xi)S(\xi,\vec{\Omega})+I_o^d(z,\vec{\Omega},\vec{\Omega}_0), \quad \mu<0 \\ \bar{I}_d(z,\vec{\Omega})=-\dfrac{\sigma(\vec{\Omega})}{|\mu(\vec{\Omega})|}\displaystyle\int_z^H p(\xi)U_d(\xi,\vec{\Omega})d\xi+\dfrac{1}{|\mu(\vec{\Omega})|} \\ \qquad \times\displaystyle\int_z^H p(\xi)S(\xi,\vec{\Omega})+I_H^d(z,\vec{\Omega},\vec{\Omega}_0), \quad \mu>0 \\ \text{where:} \\ \quad S(\xi,\vec{\Omega})=\displaystyle\int_{4\pi}\sigma_s(\vec{\Omega}'\to\vec{\Omega})U_d(\xi,\vec{\Omega}')d\vec{\Omega}', \\ I_o^d(z,\vec{\Omega},\vec{\Omega}_0)=\dfrac{f_{\mathrm{dir}}(\lambda,\vec{\Omega}_0)\sigma_s(\vec{\Omega}_0\to\vec{\Omega})}{|\mu(\vec{\Omega})\mu(\vec{\Omega}_0)|}\displaystyle\int_0^H p(\xi)U_\delta(\xi)d\xi \\ \qquad +[1-f_{\mathrm{dir}}(\lambda,\vec{\Omega}_0)]d(\vec{\Omega},\vec{\Omega}_0), \quad \mu<0 \\ I_H^d(z,\vec{\Omega},\vec{\Omega}_0)=\dfrac{f_{\mathrm{dir}}(\lambda,\vec{\Omega}_0)\sigma_s(\vec{\Omega}_0\to\vec{\Omega})}{|\mu(\vec{\Omega})\mu(\vec{\Omega}_0)|} \\ \qquad \times\displaystyle\int_z^H p(\xi)U_\delta(\xi)d\xi+I_H(\vec{\Omega}), \quad \mu>0 \end{cases} \tag{57}$$

It is interesting to note that formula for $\bar{I}(z,\vec{\Omega})$ [Eq. (57)] is similar to the system of equation for $U(z,\vec{\Omega})$ [Eq. (54)]. The following important property of the equation for $U(z,\vec{\Omega})$ and $\bar{I}(z,\vec{\Omega})$ is valid if and only if [see Eq. (58)]

$$q(z,\xi,\vec{\Omega})=p(z)\cdot p(\xi) \tag{58}$$

which results in Eq. (59):

$$K(z,\xi,\vec{\Omega})=\frac{q(z,\xi,\vec{\Omega})}{p(z)}\equiv\frac{p(z)\cdot p(\xi)}{p(z)}=p(\xi) \tag{59}$$

then the equations for $U(z,\vec{\Omega})$ and $\bar{I}(z,\vec{\Omega})$ are identical. This means that the mean intensity over the vegetated area is equal to the mean intensity over the whole space. This corresponds to the turbid medium case where there is no correlation between the distribution of vegetated spaces in the canopy.

Another important note about the system of equations for the mean field: the equations do not describe the hot-spot effect. This is also true for the classical stochastic equation [Eq. (13)]. Numerical simulations (described later) attest to this. Thus, we use the standard approach to implement the hot spot; that is, to modify the extinction coefficient, $\sigma(\vec{\Omega})$.

## VEGETATION CANOPY ENERGY BALANCE

The results obtained earlier for the mean intensity are necessary for the analysis of energy fluxes in vegetation canopies. The standard procedure to trace the energy input and output to and from the system is to integrate the equation for the mean intensity [Eq. (57)] over the canopy space and over all directions. The resulting equation describes the energy conservation law, Eqs. (60) and (61):

$$A+R+[1-\rho_{\text{soil}}(\lambda)]\cdot T=1 \quad \text{(general problem)} \tag{60}$$

$$A_i+R_i+T_i=1 \quad (i=\text{BS or S problem}) \tag{61}$$

where $A$ is absorptance, $R$ is reflectance, and $T$ is transmittance for the general problem, defined by Eq. (13) and Eq. (17) or Eq. (54) and Eq (57); $A_i$, $R_i$, and $T_i$ represent the same as for BS and S problems. As mentioned earlier, the solution of the general problem can be expressed through BS and S problems [see Eq. (24) through Eq. (27)], so we need to give the final expressions only for $A_i$, $R_i$, and $T_i$. In the case of BS problem these quantities are [see Eq. (62), (63), and (64)]

$$A_{\text{BS}}(\lambda)=[1-\omega(\lambda)]\left\{\int_0^H d\xi\int_{4\pi} d\vec{\Omega}p(\xi)\sigma(\vec{\Omega})U_d(\xi,\vec{\Omega}) + \frac{f_{\text{dir}}(\lambda,\vec{\Omega}_0)\sigma(\vec{\Omega}_0)}{|\mu(\vec{\Omega}_0)|}\int_0^H p(\xi)U_\delta(\xi)d\xi\right\} \tag{62}$$

$$R_{\text{BS}}(\lambda)=\int_{2\pi^+}\bar{I}_d(0,\vec{\Omega})|\mu(\vec{\Omega})|d\vec{\Omega} \tag{63}$$

$$T_{\text{BS}}(\lambda)=\int_{2\pi^-}\bar{I}_d(H,\vec{\Omega})|\mu(\vec{\Omega})|d\vec{\Omega}+f_{\text{dir}}(\lambda,\vec{\Omega}_0)\bar{I}_\delta(H) \tag{64}$$

and for the S problem [see Eqs. (65), (66), and (67)]

$$A_s(\lambda)=[1-\omega(\lambda)]\int_0^H d\xi\int_{4\pi} d\vec{\Omega}p(\xi)\sigma(\vec{\Omega})U_d(\xi,\vec{\Omega}) \tag{65}$$

$$R_s(\lambda)=\int_{2\pi^-}\bar{I}_d(H,\vec{\Omega})|\mu(\vec{\Omega})|d\vec{\Omega} \tag{66}$$

$$T_s(\lambda)=\int_{2\pi^+}\bar{I}_d(0,\vec{\Omega})|\mu(\vec{\Omega})|d\vec{\Omega} \tag{67}$$

Note that absorptance for both problems is different from that of the turbid medium; that is, the absorptance is expressed not through the mean intensity over the total space, $\bar{I}(z,\vec{\Omega})$, but through the mean intensity over the vegetated area, $U(z,\vec{\Omega})$. This is due to the fact that energy can be absorbed only by foliage elements, but not by voids between leaves (or between trees). One can compare this result with that for the turbid medium, taking the BS problem as an example [see Eq. (68)]

$$\begin{aligned}A&=\int_0^H d\xi\int_{4\pi} d\vec{\Omega}\sigma_a(\vec{\Omega})\bar{I}(\xi,\vec{\Omega})\\&=[1-\omega(\lambda)]\int_0^H d\xi\int_{4\pi} d\vec{\Omega}\sigma(\vec{\Omega})\bar{I}(\xi,\vec{\Omega})\\&=[1-\omega(\lambda)]\left\{\int_0^H d\xi\int_{4\pi} d\vec{\Omega}\sigma(\vec{\Omega})\bar{I}_d(\xi,\vec{\Omega}) + \frac{f_{\text{dir}}(\lambda,\vec{\Omega}_0)\cdot\sigma(\vec{\Omega}_0)}{|\mu(\vec{\Omega}_0)|}\int_0^H\bar{I}_\delta(\xi)d\xi\right\}\end{aligned} \tag{68}$$

The new formula for absorptance can be derived starting with its physical definition [see Eq. (69)]

$$A\equiv\frac{\int\int_{V4\pi} I(r,\vec{\Omega})\chi(\vec{r})\sigma(\vec{\Omega})d\vec{r}\,d\vec{\Omega}}{\int\int_{S_{2\pi^-}} I(z=0,x,y,\vec{\Omega})|\mu(\vec{\Omega})|dxdyd\vec{\Omega}} \tag{69}$$

Assuming that the incident radiant energy is normalized to unity, as in Eq. (70):

$$\int_{\pi R^2}\int_{2\pi^-} I(z=0,x,y,\vec{\Omega})|\mu(\vec{\Omega})|dxdyd\vec{\Omega}=\pi R^2 \tag{70}$$

the correct expression for absorptance is as shown in Eq. (71):

$$\begin{aligned}A&=\frac{1}{\pi R^2}\int\int_{V4\pi} I(r,\vec{\Omega})\chi(\vec{r})\sigma(\vec{\Omega})d\vec{r}\,d\vec{\Omega}\\&=\frac{1}{\pi R^2}\int_0^H dz\int_{4\pi} d\vec{\Omega}\int_{4\pi R^2}\chi(\vec{r})\sigma(\vec{\Omega})I(\vec{r},\vec{\Omega})dxdy\\&=\int_0^H dz\int_{4\pi} d\vec{\Omega}p(z)\sigma(\vec{\Omega})U(z,\vec{\Omega})\end{aligned} \tag{71}$$

Note, in the above we have used the limit from Eq. (30) [see Eq. (72)]

$$\lim_{R\to\infty}\frac{1}{\pi R^2}\int\int_{S_R} I(x,y,z,\vec{\Omega})\chi(x,y,z)dxdy=p(z)U(z,\vec{\Omega}) \tag{72}$$

Finally, the new formulation of absorbtance for a general discontinuous case collapses to the standard turbid medium definition if [see Eq. (73)]

$$K(z,\xi,\vec{\Omega})\equiv\frac{q(z,\xi,\vec{\Omega})}{p(z)}=\frac{p(z)\cdot p(\xi)}{p(z)}=p(\xi) \tag{73}$$

This formula expresses the absence of correlation between vegetated elements located at $z$ and $\xi$.

## NUMERICAL SOLUTION OF THE MEAN RTE

To solve the system of integral equations for mean intensities $U(z,\vec{\Omega})$ [Eqs. (53) and (54)] and $\bar{I}(z,\vec{\Omega})$ [Eqs. (56) and (57)], a model of the vegetation canopy structure is required, together with a numerical scheme for solution of the corresponding transfer equations. Important variables in the equations for mean intensities are the function $p(z)$ and $K(z,\xi,\vec{\Omega})$, which can be obtained from a model of the canopy structure. Note that $p(z)$ is the probability of finding a vegetated area in a horizontal plane at depth $z\in[0;H]$ and $K(z,\xi,\vec{\Omega})$ is the conditional probability of the presence of vegetated areas in planes $z$ and $\xi$, where $z,\xi\in[0;H]$. We used a simple model of

a vegetation canopy by representing the plants or trees as parallelepipeds distributed on the ground with probability $p(H)$. Further, they do not overlap, and they all have the same dimensions (height, width, and depth), and $p(z)$=const=$p(H)$ is equal to the portion of the plane covered by vegetation. Function $K(z,\xi,\vec{\Omega})$ was calculated by implementing the definition of $K(z,\xi,\vec{\Omega})$ [Eq. (37)]. When modeling the vegetation, the important question about choosing elementary volume/pixel size arises. It is probably of little interest to reproduce all these random fluctuations on BRF shape. The area of averaging (pixel size) should cover the community of vegetation (forest/field) to remove these random fluctuations. The case in our model of vegetation was a community of randomly located parallelepipeds representing trees/shrubs. This model does not give the hot spot. But there is still a problem of choosing physical elementary volume, which can be found in all integrals of mean RTE. This should be done at the level of leaf aggregates.

In the system of integral equations for $\bar{I}(z,\vec{\Omega})$ and $U(z,\vec{\Omega})$, one needs to solve only the system for $U(z,\vec{\Omega})$. The evaluation of $\bar{I}(z,\vec{\Omega})$ is a straightforward numerical integration of $U(z,\vec{\Omega})$. To solve the system for $U(z,\vec{\Omega})$, the method of successive orders of scattering approximations (SOSA) was used (Myneni et al., 1987). The $n$th approximation to the solution is given by Eq. (74):

$$U_d^n(z,\vec{\Omega})=J_1(z,\vec{\Omega})+J_2(z,\vec{\Omega})+\ldots+J_n(z,\vec{\Omega}) \tag{74}$$

The functions $J_k(z,\vec{\Omega})$, $k=1, 2, \ldots, n$ are the solutions of the system of two independent equations [see Eq. (75) and (76)]:

$$J_k(z,\vec{\Omega})+\frac{\sigma(\vec{\Omega})}{|\mu(\vec{\Omega})|}\int_0^z K(z,\xi,\vec{\Omega})J_k(\xi,\vec{\Omega})d\xi=R_{k-1}(z,\vec{\Omega}),\quad \mu<0 \tag{75}$$

$$J_k(z,\vec{\Omega})+\frac{\sigma(\vec{\Omega})}{|\mu(\vec{\Omega})|}\int_z^H K(z,\xi,\vec{\Omega})J_k(\xi,\vec{\Omega})d\xi=R_{k-1}(z,\vec{\Omega}),\quad \mu>0 \tag{76}$$

where [see Eq. (77)]

$$R_0(z,\vec{\Omega})=\frac{f_{\text{dir}}(\lambda,\vec{\Omega}_0)\sigma_S(\vec{\Omega}_0\rightarrow\vec{\Omega})}{|\mu(\vec{\Omega})\mu(\vec{\Omega}_0)|}\int_0^z K(z,\xi,\vec{\Omega})U_\delta(\xi,\vec{\Omega})d\xi + [1-f_{\text{dir}}(\lambda,\vec{\Omega}_0)]d(\vec{\Omega},\vec{\Omega}_0),\quad \mu<0$$

$$R_0(z,\vec{\Omega})=\frac{f_{\text{dir}}(\lambda)\sigma_S(\vec{\Omega}_0\rightarrow\vec{\Omega})}{|\mu(\vec{\Omega})\mu(\vec{\Omega}_0)|}\times\int_z^H K(z,\xi,\vec{\Omega})U_\delta(\xi,\vec{\Omega})d\xi+I_H(\vec{\Omega},\vec{\Omega}_0),\quad \mu>0$$

$$R_k(z,\vec{\Omega})=\frac{1}{|\mu(\vec{\Omega})|}\int_0^z K(z,\xi,\vec{\Omega})S_k(\xi,\vec{\Omega})d\vec{\Omega},\quad \mu<0,\ \text{when } k\geq 1$$

$$R_k(z,\vec{\Omega})=\frac{1}{|\mu(\vec{\Omega})|}\int_z^H K(z,\xi,\vec{\Omega})S_k(\xi,\vec{\Omega})d\vec{\Omega},\quad \mu>0,\ \text{when } k\geq 1 \tag{77}$$

and the source function $S(z,\vec{\Omega})$ is $S_k(z,\vec{\Omega})=\int_{4\pi}\sigma_S(\vec{\Omega}'\rightarrow\vec{\Omega})J_k(z,\vec{\Omega}')d\vec{\Omega}$.

The algorithm to solve the system of equations for $U(z,\vec{\Omega})$ is as follows: (1) Find $U_\delta(z,\vec{\Omega})$ from the corresponding Volterra equation [Eq. (53)]; (2) Evaluate $R_0(z,\vec{\Omega})$; (3) Solve the Volterra equations [Eqs. (75) and (76)] with $R_0(z,\vec{\Omega})$ and find $J_1(z,\vec{\Omega})$; (4) Evaluate $S_1(z,\vec{\Omega})=\int_{4\pi}\sigma_s(\vec{\Omega}'\rightarrow\vec{\Omega})J_1(z,\vec{\Omega}')d\vec{\Omega}'$ with $J_1(z,\vec{\Omega})$; (5) Evaluate $R_1(z,\vec{\Omega})$; (6) Calculate $J_2(z,\vec{\Omega})$; (7) Repeat the following until $\|J_n(z,\vec{\Omega})\|\leq\varepsilon$: (a) Evaluate $S_k(z,\vec{\Omega})$; (b) Calculate $R_k(z,\vec{\Omega})$; (c) Calculate $J_{k+1}(z,\vec{\Omega})$.

The numerical method used to solve the basic equations is as follows. We start with the parametric Volterra equation [Eq. (78)]

$$U(z,\vec{\Omega})+\frac{\sigma(\vec{\Omega})}{|\mu(\vec{\Omega})|}\int_0^z K(z,\xi,\vec{\Omega})U(\xi,\vec{\Omega})d\xi=F(z,\vec{\Omega}) \tag{78}$$

Here $\vec{\Omega}$ is a parameter of the equation. The corresponding discrete scheme is shown in Eq. (79)

$$U(k,\vec{\Omega})+\frac{\sigma(\vec{\Omega})}{|\mu(\vec{\Omega})|}\sum_{j=1}^{i=k}W_{kj}K(k,j,\vec{\Omega})U(j,\vec{\Omega})=F(k,\vec{\Omega}) \tag{79}$$

where $W_{kj}$ is the weight, which depends on the numerical scheme used for approximating the integral. Then, $U(1,\vec{\Omega})=F(1,\vec{\Omega})$, when $k=1$, and when $k\in[2,N_z+1]$ [see Eq. (80)]

$$U(k,\vec{\Omega})+\frac{\sigma(\vec{\Omega})}{|\mu(\vec{\Omega})|}W_{kk}K(k,k,\vec{\Omega})U(k,\vec{\Omega}) =F(k,\vec{\Omega})-\frac{\sigma(\vec{\Omega})}{|\mu(\vec{\Omega})|}\sum_{j=1}^{j=k-1}W_{kj}K(k,j,\vec{\Omega})U(j,\vec{\Omega}), \tag{80}$$

$$\Rightarrow U(k,\vec{\Omega})=\frac{F(k,\vec{\Omega})-\frac{\sigma(\vec{\Omega})}{|\mu(\vec{\Omega})|}\sum_{j=1}^{i=k-1}W_{kj}K(k,j,\vec{\Omega})U(j,\vec{\Omega})}{1+\frac{\sigma(\vec{\Omega})}{|\mu(\vec{\Omega})|}W_{kk}K(k,k,\vec{\Omega})} \tag{81}$$

Another important method used in this algorithm is the method of $S_n$ quadratures of Carlson (Bass et al., 1986) to evaluate angular integrals. This scheme belongs to the method of Gauss quadratures. The quadrature is built as follows. The octant is divided into $n\cdot(n+2)/8$ parts of equal area, $w_0=4\pi/n\cdot(n+2)$ using latitudes, defined as $\mu=\mu_{\ell+1/2}$, $\ell=0, 1, \ldots, \frac{n}{2}$ and longitudes, defined as $\varphi=\varphi_{\ell,m+1/2}$, $m=0, 1, \ldots, \frac{n}{2}-\ell+1$. The coordinates of the boundaries of each layer are shown in Eq. (82):

$$\mu_{\ell\pm1/2}=1-\frac{(n-2\ell+2)\cdot[n-2(\ell-1\pm1)]}{n\cdot(n+2)} \tag{82}$$

and the coordinates of the centers of layers are shown in Eq. (83)

$$\bar{\mu}_\ell = 1 - \frac{[n-2\ell+2]^2}{n\cdot(n+2)} \tag{83}$$

The nodes of quadratures are shown in Eq. (84)

$$\begin{cases} \mu_\ell = \bar{\mu}_\ell + f\cdot\mu_{\ell-1/2}, & \ell = 0,1,\ldots,\dfrac{n}{2} \\ \varphi_{\ell,m} = \dfrac{\pi}{2}\left[\dfrac{2m-1}{n-2\ell+2}A_n + \dfrac{1}{2}(1-A_n)\right], & m = 1,2,\ldots,\dfrac{n}{2}-\ell+1 \end{cases} \tag{84}$$

and the coefficient $f$ and $A_n$ are determined from condition to give exact expressions for spherical integrals with integrand function 1, $\mu$ and $\mu^2$.

Generally, about 30 iterations are sufficient to obtain a relative accuracy of $10^{-3}$. The physical interpretation of the method of successive orders is obvious: the function $J_k(z,\vec{\Omega})$ is the mean radiance of photons scattered $k$ times. The rate of convergence of this method, $\rho_c$, has been defined by Vladimirov (1963) and Marchuk and Lebedev (1971) as shown in Eq. (85):

$$\|I - I_n\| \leq \rho_c = [1-\exp(-k_0\cdot H)]\cdot\eta\cdot n \tag{85}$$

where $k_0$ is a certain coefficient and effective single scattering albedo $\eta$ [see Eq. (86)]:

$$\eta = \sup_{0<z<H}\ \sup_{\Omega\in 4\pi}\frac{\sigma_S(\vec{\Omega}_0\rightarrow\vec{\Omega})}{\sigma(z,\vec{\Omega})} \tag{86}$$

From Eq. (85) it follows that SOSA should be used in the case of small optical depth of the layer or in the case of small $\eta$. If $\eta\approx 1$ and the optical depth is large, the method becomes tedious.

## EVALUATION OF THE MODEL

To illustrate the characteristics of the model of mean RTE described here, the numerical results of the calculations of important quantities, such as directional reflectance (BRF) in the principal plane, and energetic quantities [absorbtance, transmittance, reflectance (DHR/BHR)] are presented in this section. The input variables of Mean RTE model are: (1) solar illumination variables—solar angle $\vec{\Omega}_0$ and the ratio of direct-to-total incident flux; (2) canopy geometry, including height $H$, and horizontal dimensions of individual vegetation units (trees, shrubs), $d$; (3) statistical moments of the ensemble of vegetation units, namely, functions $p(z)$ and $K(z,\xi,\vec{\Omega})$ defined earlier by Eqs. (36) and (37); (4) characteristics of leaves—density of leaves $u_L(\vec{r})$, leaf normal orientation distribution (uniform, planophile, erectophile, etc; Ross, 1975), hemispherical reflectance, and transmittance spectra of leaves $r_D(\lambda)$, $t_D(\lambda)$; and, (5) soil hemispherical reflectance spectra $\rho_{\text{soil}}(\lambda)$. Model outputs are (1) the directional reflectance or the bidirectional reflectance factors (BRF) defined as the surface-leaving radiance, divided by radiance from a conservation Lambertian reflector under monodirectional illumination (Knyazikhin et al., 1998b) [see Eq. (87)]:

$$\text{BRF} = \frac{I_\lambda(\vec{r}_{\text{top}},\vec{\Omega},\vec{\Omega}_0)}{1/\pi\int_{2\pi^-} I_\lambda(\vec{r}_{\text{top}},\vec{\Omega},\vec{\Omega}_0)|\vec{\Omega}\cdot\vec{n}_{\text{top}}|d\vec{\Omega}} \tag{87}$$

and (2) absorbtance, transmittance, and reflectance. We calculate two types of hemispherical reflectance, BHR and DHR, defined as follows: The bihemispherical reflectance (BHR) for nonisotropic incident radiation (both direct and diffuse components) is the ratio of the mean radiant exitance to the incident radiance (Knyazikhin et al., 1998b) [see Eq. (88)]

$$\text{BHR} = \frac{\int^{2\pi^+} I_\lambda(\vec{r}_{\text{top}},\vec{\Omega},\vec{\Omega}_0)|\vec{\Omega}\cdot\vec{n}_{\text{top}}|d\vec{\Omega}}{\int_{2\pi^-} I_\lambda(\vec{r}_{\text{top}},\vec{\Omega},\vec{\Omega}_0)|\vec{\Omega}\cdot\vec{n}_{\text{top}}|d\vec{\Omega}} \tag{88}$$

and the directional hemispherical reflectance (DHR) is defined similar to BHR, except that the incident radiation has only the direct component. Below, we present the results of comparison of the model of Mean RTE with similar RT models, with Monte Carlo simulations of the radiation field in a maize canopy and with field data from Jornada PROVE. Issues related to the effect of vegetation clumping on the radiation regime are discussed later.

The 3-D dynamic architecture model of maize proposed by España et al. (1999) was utilized for Monte Carlo simulations. This model allows the description of the maize canopy from emergence to male anthesis. Because maize is planted in rows and for each vegetation unit the leaves are obviously clumped around the stem, the assumption of a random leaf spatial distribution is not valid. The driving parameter of the model is the phenological stage, which is defined by the number of leaves produced since emergence and not totally hidden in the top leafy cone. The model describes the dynamics of the dimensions, height, senescence, curvature, and insertion angle of the leaves, as well as the temporal evaluation of the stem dimensions. Linear equations were developed to describe the growth of the leaf size, stem diameter with change of leaf stage, and so on. The inputs to the 3-D model are: (1) leaf stage (which describes time); (2) plant density, including seeding pattern (row spacing and orientation, plant spacing); (3) leaf area cumulated over the fully developed plant, including leaves that senesced; and (4) final height of the canopy. The maize canopy architecture model was calibrated and validated with three sets of experiments, two of which were performed in Avignon, France (INRA-90, plant density of 12, plants·m$^{-2}$, canopy measured when the fourteenth leaf appeared, and INRA-97, plant density of 8.5 plants·m$^{-2}$, measurements performed at two phenological stages, namely, 13 and 17 leaves). The third experiment was performed in Alpilles, France (Alpilles-97 plant density

*Table 1.* Physical Characteristics of six Growth Stages of Maize Canopy

| *Phenological Stage* | *Leaf Stage* | *LAI* | *Plant Height (m)* | *Cover Fraction* |
|---|---|---|---|---|
| 1 | 4 | 0.25 | 0.085 | 0.06 |
| 2 | 8 | 0.86 | 0.195 | 0.19 |
| 3 | 12 | 1.64 | 0.407 | 0.35 |
| 4 | 16 | 2.34 | 0.820 | 0.45 |
| 5 | 18 | 3.01 | 1.800 | 0.55 |
| 6 | 24 | 6.25 | 2.200 | 1.00 |

From España (in press).

of 7 plants·m$^{-2}$, measurements performed when the fifteenth leaf was appearing).

The maize canopy was simulated using computer graphic techniques as an assembly of leaves and stems. Six phenological stages of the maize canopy were simulated, corresponding to LAI values of 0.25, 0.86, 1.64, 2.34, 3.01, and 6.25 (Table 1). Optical properties of the leaves were determined at three chlorophyll *a* and *b* concentrations, Cab30, Cab50, and Cab70, which corresponded to 30, 50, and 70 $\mu$g·cm$^2$ concentrations of chlorophyll *a* and *b*. The optical properties for the case of Cab50 were used in our validation studies (Table 2).

Dry and wet soils with corresponding optical properties were considered (Baghdadi, 1998). Soil reflection was assumed to be Lambertian; soil hemispherical reflectances are given in Table 2. To validate the Mean RTE method, results of simulations from a Monte Carlo raytracing method in a maize canopy were utilized (Baghdadi, 1998; España et al., 1999). A total of three million photons were simulated. The incoming photon flux, corresponding to direct solar illumination, was constrained to have a constant zenith angle of 45°, and 150 azimuthal directions were simulated (in intervals of 2.4°, where 0° corresponds to the direction perpendicular to the rows). Each of these 150 directions was simulated using twenty thousand photons. There were 360×90=32,400 viewing directions (steps of 1° along both the zenith and azimuth). The simulations were carried out at 10 wavelengths: 430, 500, 562, 630, 692, 710, 740, 795, 845, and 882 nm.

The model of mean RTE was run with the same set of input parameters. It is interesting to compare the CPU time required to run both models. The Monte Carlo model requires a maximum of 48 hours to generate radiances for the whole spectra at all azimuthal directions on a SUN 20 workstation. The CPU consumption of mean RTE is highly dependable on the value of LAI and leaf albedo $\omega(\lambda)$. For small LAI (<3) and small leaf albedo (<0.7) it takes up to 5 minutes to generate radiances at 40 directions of quadrature for the upper hemisphere on an SGI O2 workstation. If both LAI and $\omega(\lambda)$ are high [LAI>8, $\omega(\lambda)$>0.95], it can take up to 45 minutes, because we should significantly decrease the step of discritization.

Figures 3, 4, and 5 present the results of comparison. We should note that not all of the parameters required to parameterize the model of Mean RTE were available; for example, ground cover and horizontal dimensions of maize leaves were not available. Therefore, these parameters were estimated from description of the maize canopy, or in some cases interpolated using available data. Figure 3 shows simulations of the BRF in the principal plane for the case of dry soil, chlorophyll concentration of 50 $\mu$g·cm$^2$ (Cab50) at RED (630 nm) and NIR (845 nm) wavelengths, and for three LAI values—low (LAI=0.86), intermediate (LAI=2.34), and high (LAI=6.25). Other parameters are listed in Table 1. The incoming radiation was a monodirectional flux with a polar angle of 45°. In Figure 3, it can be seen that the characteristic shape of BRF changes dramatically from an inverted bowl to a bowl shape. This provides an opportunity to validate the Mean RTE model.

Using simple physics, we can explain the changes in radiance. The following formulas cannot be considered as asymptotic ones, and they do not consider complex phenomenon such as the hot spot. They represent qualitative analysis. When the total amount of radiation reflected by the vegetation back to the atmosphere is higher than that reflected by bare soil under the canopy, the BRF will have a characteristic bowl shape and the measured quantity, the radiance is [see Eq. (89).

$$I(\theta,\varphi)\sim\frac{\Phi}{\Omega\cdot A\cdot\cos(\theta)} \tag{89}$$

here $\Phi$ denotes flux, $\Omega$ the solid angle, and $A$ is an area of surface emanating from this flux in direction $\vec{\Omega}$. This formula is a definition of radiance using the standard notion of flux. Because of the chaoticity of distribution of

*Table 2.* Optical Properties of the Maize Leaves and the Soil

| | *Wavelength, nm* | | | | | | | | | |
|---|---|---|---|---|---|---|---|---|---|---|
| | *430* | *500* | *562* | *630* | *692* | *710* | *740* | *795* | *845* | *882* |
| Leaf refl., Cab50 | 0.0512 | 0.0636 | 0.1403 | 0.0798 | 0.0646 | 0.2248 | 0.4222 | 0.4574 | 0.4581 | 0.458 |
| Leaf trans., Cab50 | 0.0086 | 0.04 | 0.1526 | 0.0791 | 0.0557 | 0.2625 | 0.4787 | 0.5185 | 0.5187 | 0.519 |
| Dry soil hem. refl. | 0.1118 | 0.1359 | 0.1657 | 0.1976 | 0.2192 | 0.2262 | 0.2399 | 0.2579 | 0.2720 | 0.2794 |
| Moist soil hem. refl. | 0.0469 | 0.0557 | 0.0673 | 0.0825 | 0.0943 | 0.0983 | 0.1064 | 0.1177 | 0.1268 | 0.1316 |

From España (in press). Cab50 designates chlorophyll *a* and *b* concentration of 0.5 g·m$^2$.

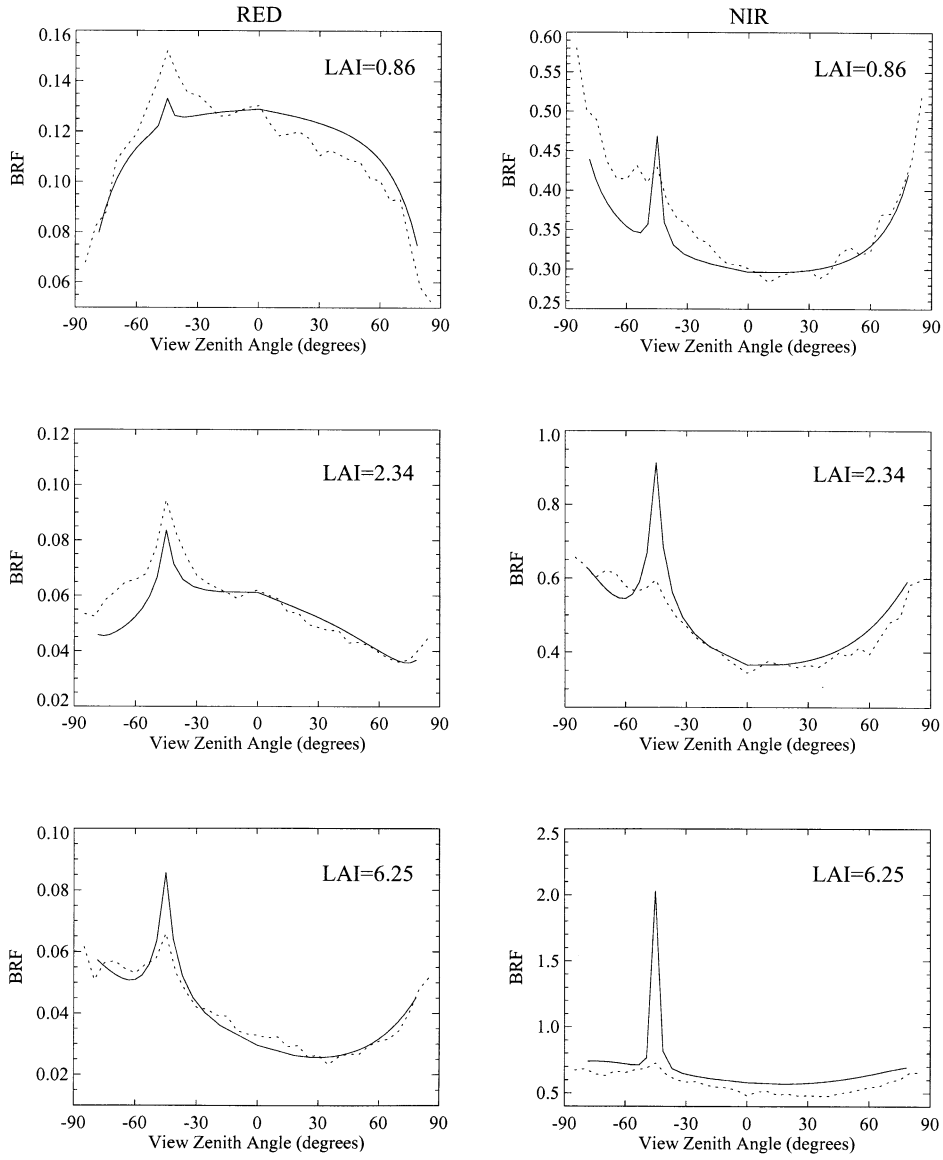


*Figure 3.* Comparison of BRF in the principal plane simulated by Mean RTE (solid line) and Monte Carlo (dashed line) methods. In all cases soil is "dry," Cab=50, and SZA=45°.

reflecting elements (leafs) along all directions, the flux $\Phi$ has a weak angular dependence; thus $I(\theta,\varphi)$ changes with $\theta$ as $\cos(\theta)^{-1}$. The situation is similar to the distributed isotropic energy sources on the top of the canopy. In contrast to this case, there is significant contribution to BRF from isotropic sources located on the soil surface, when vegetation is sparse and soil reflection predominates. In this case, the above formula is applicable not to the top of canopy, but to the soil surface. But before the radiation emitted by the surface will reach the top of the canopy, it will be attenuated by a factor $\exp[-a/\cos(\theta)]$ (Beer's law, where $a$ is some characteristic coefficient of media). Thus, we have Eq. (90):

$$I(\theta,\varphi)\sim\frac{\Phi\cdot\exp[-a/\cos(\theta)]}{\Omega\cdot A\cdot\cos(\theta)} \qquad (90)$$

where results in $I(\theta,\varphi)$ decreasing as $\theta\rightarrow 90°$.

The next set of plots, Figure 4, presents validation of the estimated parameters. Here, we used the "dry soil" simulations to estimate the full set of parameters, and then we ran the Mean RTE model for case of "wet soil," changing only the soil reflectance, which was known from measurements (Baghdadi, 1998). In both cases LAI is 1.64, chlorophyll concentration of 50 $\mu$g·cm$^2$, and RED and NIR wavelengths were used. The general comment to Figure 3 and Figure 4 is that while the model of mean RTE simulates quite well most of the shapes of BRF, its performance is poorer near the direction of the hot spot, because the hot-spot model considers only single scattering. Figure 5 represents another attempt at validation of the RTE model in general and the set of estimated parameters in particular. The idea was to compare hemispherical reflectance (DHR) of the Monte Carlo methods with the mean RTE simulations, under identical set

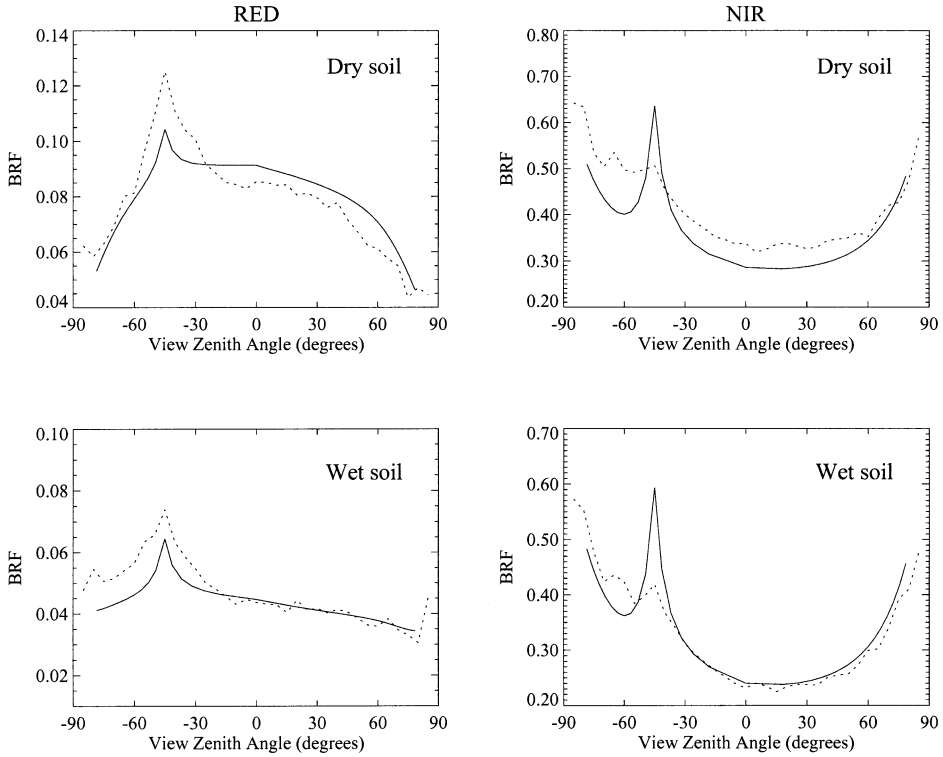


*Figure 4.* Comparison of BRF in the principal plane simulated by Mean RTE (solid line) and Monte Carlo (dashed line) methods. In all cases LAI=1.64, Cab=50, and SZA=45°. The "dry" soil case was used to estimate parameters, and the "wet" soil case was used for validation.

of parameters. We ran the Mean RTE model for the case of "wet" and "dry soil," with chlorophyll concentration of 50 $\mu g \cdot cm^2$ (Cab50) at the 10 available wavelengths (Table 1). For the case of dry soil, five values of LAI were used (LAI=0.86, 1.64, 2.34, 3.01, and 6.25), and three for the case of wet soil (LAI=1.64, 3.01, and 6.25), which results in 50 points for dry soil and 30 points for wet soil. The most significant difference (18%) is seen in NIR wavelengths, where reflectance is high, and in the case of a dense canopy (LAI of 6.25). One source of discrepancy is the numerical scheme of evaluating DHR from Monte Carlo angular intensities of at least 3%. Also, the error in the numerical solution of the transfer equation increases at NIR and in dense canopies as shown in Eq. (91)

$$\Delta I \sim \frac{1}{1-\omega(\lambda)\exp(\mathrm{LAI}\cdot k)} \tag{91}$$

The performance of the Mean RTE model was also studied in comparison to similar RTE models. We used the 1-D model (Shultis and Myneni, 1988) "TWOVEG," and the 3-D model "DISORD," which are numerical methods of solution of one- and three-dimensional radiative transfer equations in plant canopies modeled as turbid media using the discrete ordinates method. Figures 6 and 7 presents the results of comparison between the three models at two wavelengths, RED (645 nm) and NIR (841 nm). The incident radiation was 80% direct and 20% diffuse isotropic sky light, and the solar zenith angle was 30°. The soli hemispherical reflectance was set to 0, so the BS problem was studied. Only the case of

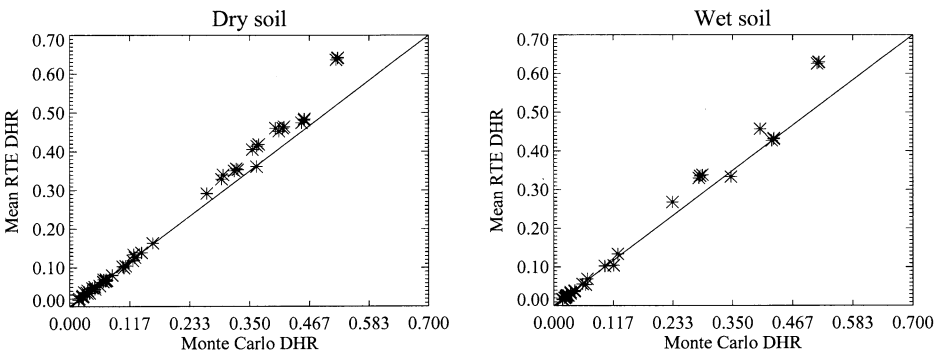


*Figure 5.* Comparison of DHR simulated by Mean RTE and Monte Carlo methods for "dry" and "wet" soil cases. Fifty values of DHR were compared in the case of "dry" soil and 30 values for "wet" soil.

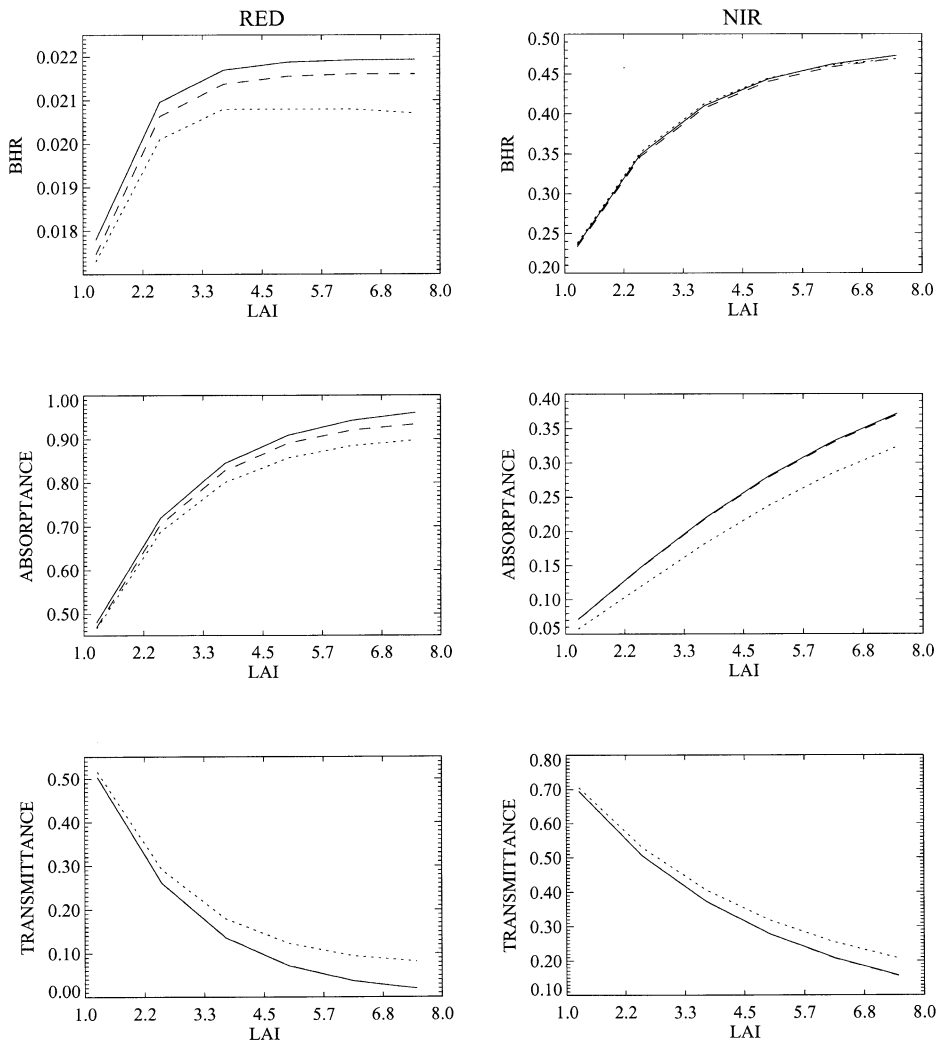


*Figure 6.* BHR, absorptance, and transmittance as a function of LAI at red (left) and near-infrared (right) wavelengths evaluated with Mean RTE (solid line), TWOVEG (dashed line), and DISORD (dotted line). In all cases SZA=30°.

a homogeneous canopy was considered, so as to include TWOVEG also in the comparison. Figure 6 presents the BHR, absorbtance, and transmittance versus LAI. All models show the general tendency of absorbtance to increase and transmittance to decrease with an increase in LAI. The increase of BHR with LAI is due to the completely absorbing soil; as LAI increases, the leaves hide this perfect absorber, and hence the increase in BHR. Figure 7 illustrates dependencies of BHR, absorbtance, and transmittance with respect to solar zenith angle at a constant LAI of 5. The general tendency of absorbtance to increase and transmittance to decrease with an increase in solar zenith angle is correct, because the path length increases as the solar zenith angle increases, and the probability of the solar rays to be intercepted also increases. Bihemispherical reflectance also increases with an increase in solar zenith angle, because at oblique sun angles, more energy is reflected from the boundary and there is correspondingly less penetration into the deepest parts of the canopy. From Figures 6 and 7 it can be seen that the largest discrepancy between model estimates is for BHR, especially between the Mean RTE and DISORD at RED, for absorbtance versus solar zenith angle at both RED and NIR, and for transmittance versus solar zenith angle at RED. This may be attributed to various simplifying approximations used in the numerical solution schemes. Nevertheless, comparison of mean RTE with the 1-D (TWOVEG) model gives good agreement, which is the more valuable result, because the 1-D model is designed specially to simulate homogeneous canopy, and we perform comparison when mean RTE also simulates a homogeneous case.

The critical validation of any model is comparison with field data. We utilized data from the Jornada field campaign distributed by the grassland PROVE (PROtotype Validation Exercise) team (Privette et al., 1999). This experiment took place from April 30 through May 13 of 1997 in Jornada (a large valley near Las Cruces, New Mexico, USA). The area is slowly undergoing a landcover change from a grassland to a shrubland (predominately mesquite). It is a very arid area, so shrubs and grasses are sparse (ground cover is 34.5±2%, average LAI~0.5).

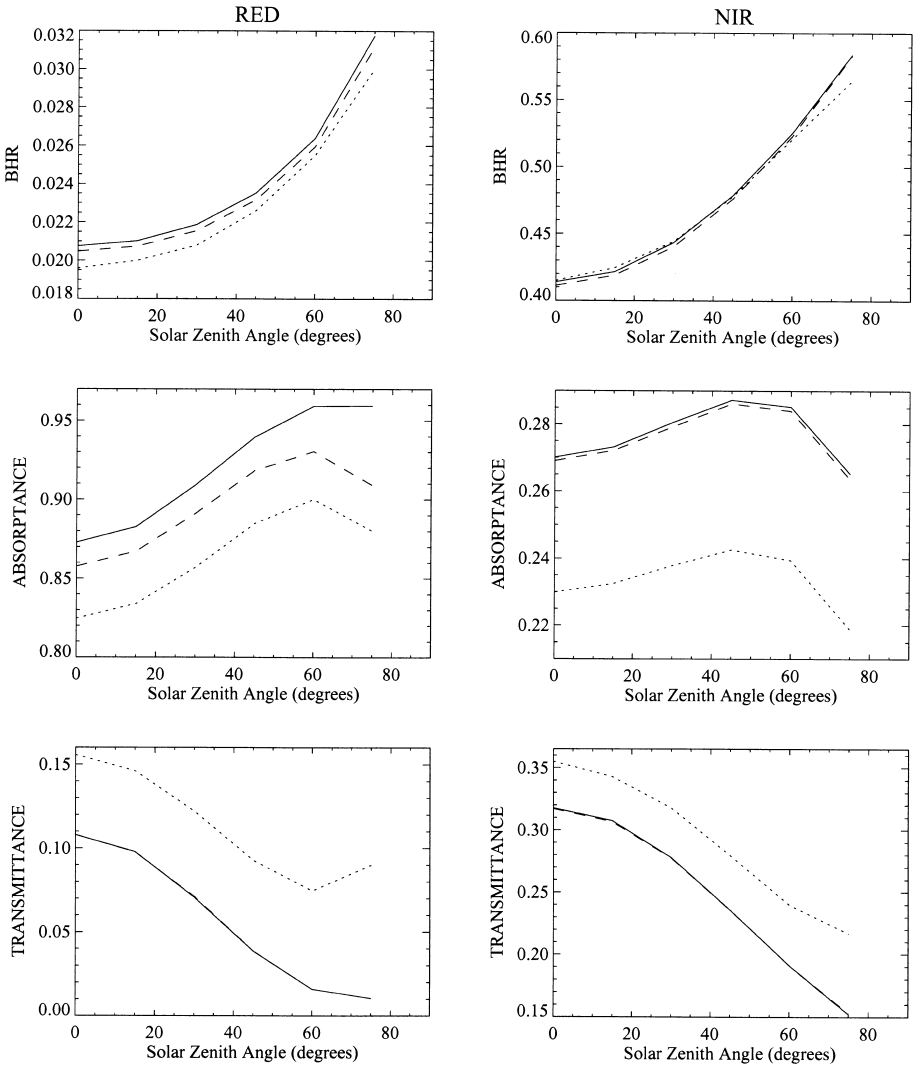


*Figure 7.* BHR, absorptance, and transmittance as a function of solar zenith angle at red (left) and near-infrared (right) wavelengths evaluated with Mean RTE (solid line), TWOVEG (dashed line), and DISORD (dotted line). Homogeneous canopy is simulated. In all cases LAI=5.

The data we used were from a transitional site (mixed grassland and shrubs) and consisted of 75% mesquite and 25% yucca and morman tea. The measurements were performed on a 26-m tall tower using a CIMEL sunphotometer, which has 4 channels. We used data from two of these channels, 870 nm and 1020 nm. Related parameters at the Jornada transition site are as follows (for mesquite): mean height, 1.28±0.54 m; LAI, 1.71; leaf reflectance at 870 mm—0.432, leaf transmittance at 870 mm—0.395; leaf reflectance at 1,020 nm—0.442; and leaf transmittance at 1,020 nm—0.399. For yucca: mean height, 0.59±0.16 m; LAI, 1.38; leaf reflectance at 870 nm—0.432; leaf transmittance at 870 nm—0.107; leaf reflectance at 1,020 nm—0.426; and leaf transmittance at 1,020 nm—0.096. Soil reflectance was 0.349 (at 870 nm) and 0.380 (at 1020 nm). We assume a Lambertian surface in our model. Figure 8 presents BRF comparisons (field data simulated by the Mean RTE) in the principal plane for three values of solar zenith angle (20°, 40°, and 70°) and at two available wavelengths (1,020 nm and 870 nm). Because the data were noisy, it was difficult to perform detailed comparison, but it appears that the agreement is reasonable. One exception is the comparison for 870 nm at SZA of 40°, where the simulated BRF is a significant overestimate. There are indications that the data may have been a problem in this instance: from other plots it is clear that the mean BRF for both channels is approximately the same at a given value of SZA. The plot under consideration is an exception.

Finally, we discuss one important feature of the model of mean RTE, which allows for description of canopy heterogeneity (i.e., mixing of voids with clusters of vegetation elements). The clustering effect has an important influence on the radiation regime in a vegetation canopy; for example, the hot-spot effect and change in the proportions of BHR, absorbtance, and transmittance. We have already mentioned that heterogeneity leads to a new analytical formula for the absorbtance, for which we must not use the mean intensity over all space, but

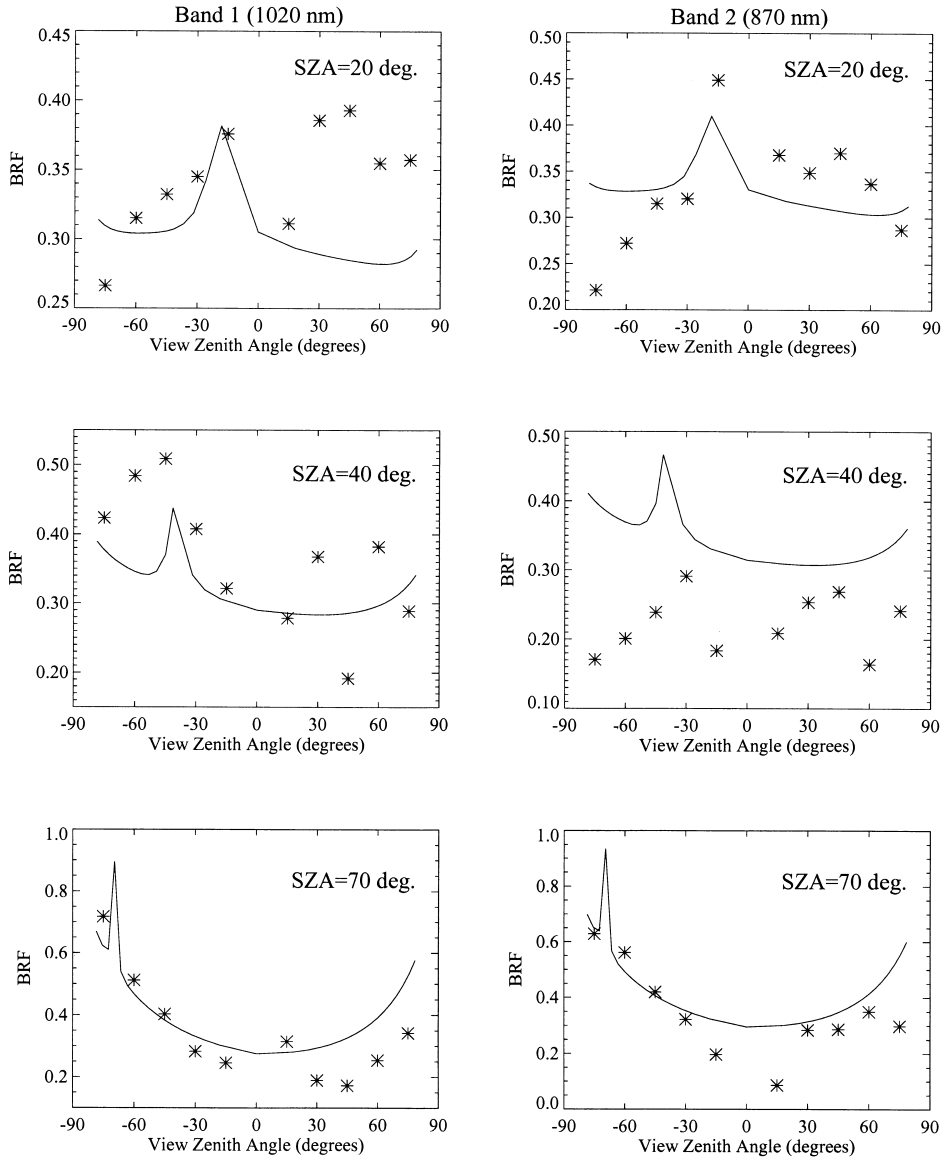


*Figure 8.* Comparison of BRF simulated by Mean RTE with Jornada PROVE field data at 1020 nm and 870 nm for three values of SZA: 20°, 40°, and 70°.

the mean intensity over only the vegetated portion of the canopy space [Eqs. (53) and (54)]. Figures 9 and 10 illustrate the influence of clumping on BHR, absorbtance, and transmittance for the case of a black soil problem and for a direct-to-total incident flux ratio of $f_{\text{dir}}(\lambda,\vec{\Omega}_0)=0.8$. To introduce voids, we varied the groundcover parameter and ran the Mean RTE for $p(z)=1.0$ (which corresponds to the turbid medium case), $p(z)=0.75$, and $p(z)=0.5$ (as $p$ decreases, clumping increases). Figure 9 presents the relationship between BHR, absorbtance, and transmittance with LAI (SZA is fixed and is equal to 30°). Figure 10 presents the same, but with changing solar zenith angle at a constant LAI of 5. The qualitative effect of voids on the radiation regime is similar at NIR and RED wavelengths. From Figure 9 it is clear that for similar input parameters, in particular LAI, but at different values of groundcover, the BHR and absorbtance decrease as groundcover decreases and transmittance increases. The same tendency is observed for BHR, absorbtance, and transmittance versus solar zenith angle (Fig. 10). The above tendency corresponds with clumping vegetation in clusters, which means increasing the amount of voids; the probability of solar radiation penetrating deep into the canopy without interactions increases, thus resulting in increased transmittance and decreased absorbtance. The quantitative effect of clumping is, for example, at LAI=3, SZA=50°, at RED, $\Delta\text{BHR} \equiv |\{\text{BHR}(p=1.0)-\text{BHR}\ (p=0.5)/\text{BHR}\ (p=\ 1.0)| \approx 42.3\%$; similarly, $\Delta\text{Absorbtance} \approx 30\%$ and $\Delta\text{Transmittance} \approx 150\%$.

## CONCLUSIONS

The main goal in this paper was to address the problem of accurately describing the influence of discontinuity in

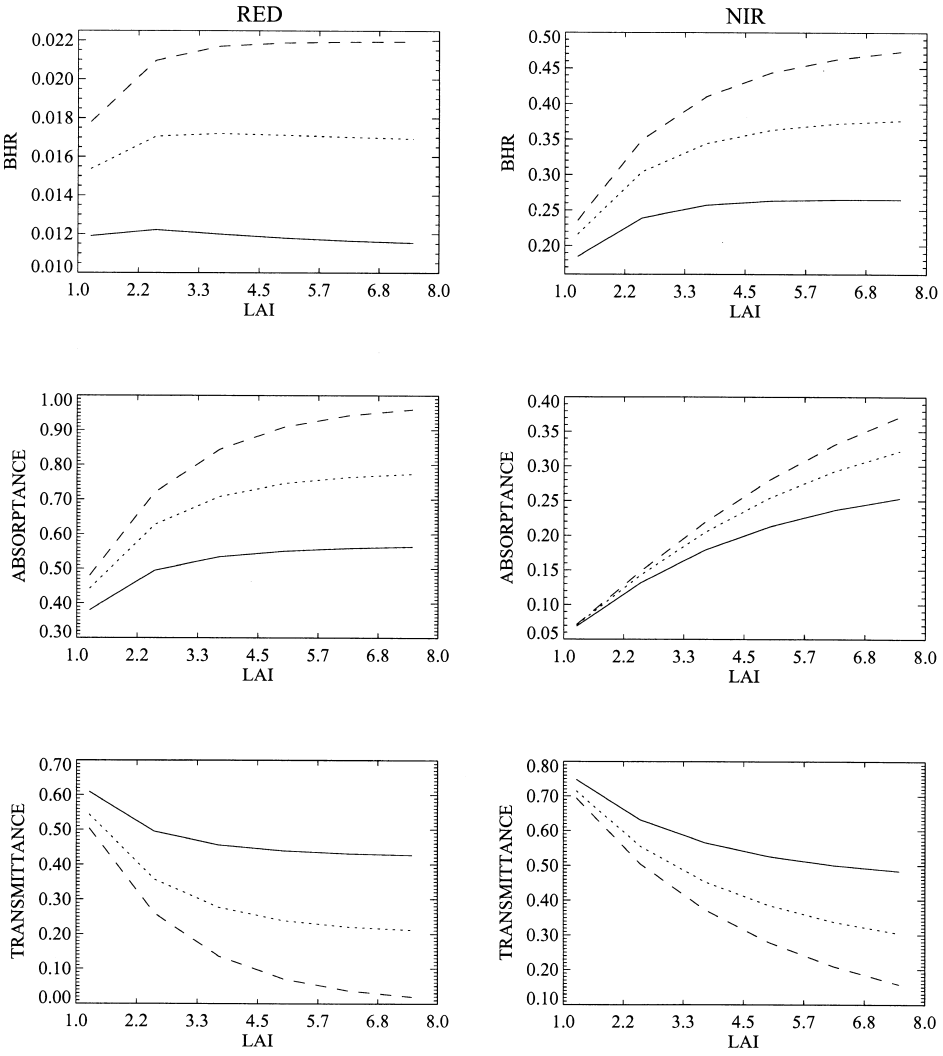


*Figure 9.* Influence of clumping on the radiation regime in vegetation canopy at red (left) and near-infrared (right) wavelengths. BHR, absorptance, and transmittance as a function of LAI evaluated at three values of groundcover, representing varying degree of clumping: $p=1.0$ (dashed line), $p=0.75$ (dotted line), $p=0.5$ (solid line). In all cases SZA=30°.

vegetation canopies on the radiative regime. The presence of gaps in vegetation canopies introduces corrections to energy fluxes, comparable to the values of fluxes for the homogeneous case, and consequently results in large errors in the retrieved biophysical parameters of vegetation, such as LAI, FPAR, etc. Among the many current models, those based on geometrical-optical approaches are valid for discontinuous vegetation canopies, but they approximate radiative fluxes and multiple scattering of photons; others, based on the classical RT equation, are accurate but applicable only to simple homogeneous cases of crops and grasses.

The proposed approach, based on a statistical formulation of RTE, is specially designed to accurately evaluate radiation fluxes in discontinuous vegetation canopies. Special attention was given to deriving analytical results. Specifically, the following major tasks were accomplished. A system of integral equations for mean field for the transport of monochromatic radiation in spatially heterogeneous canopy was formulated. The resulting system of integral equations satisfies the energy conservation law and was solved numerically using the method of successive orders of scattering approximations. The influence of discontinuity on the radiative regime in a vegetation canopy is such that a complete description of the radiation field in the canopy is possible, using not only mean radiance over the whole space, but also averages over space occupied by absorbing elements is also required. This approach allows for a correct formulation of absorbtance, which extends its classical definition for homogeneous media to nonhomogeneous cases. Using a simple model of vegetation as input to mean RTE, we studied the effect of lateral discontinuity on the relationship between BHR/absorbtance/transmittance and (1) LAI and (2) solar zenith angle. The model was validated first using similar RTE models (1-D and 3-D); second using Monte Carlo simulations in a computer-generated maize canopy; and finally, using field data from the Jornada PROVE field campaign. The general agreement is good. The major drawback of the model is an approximate description of the hot-spot effect. The numerical simulations of Mean RTE showed that this equation, as

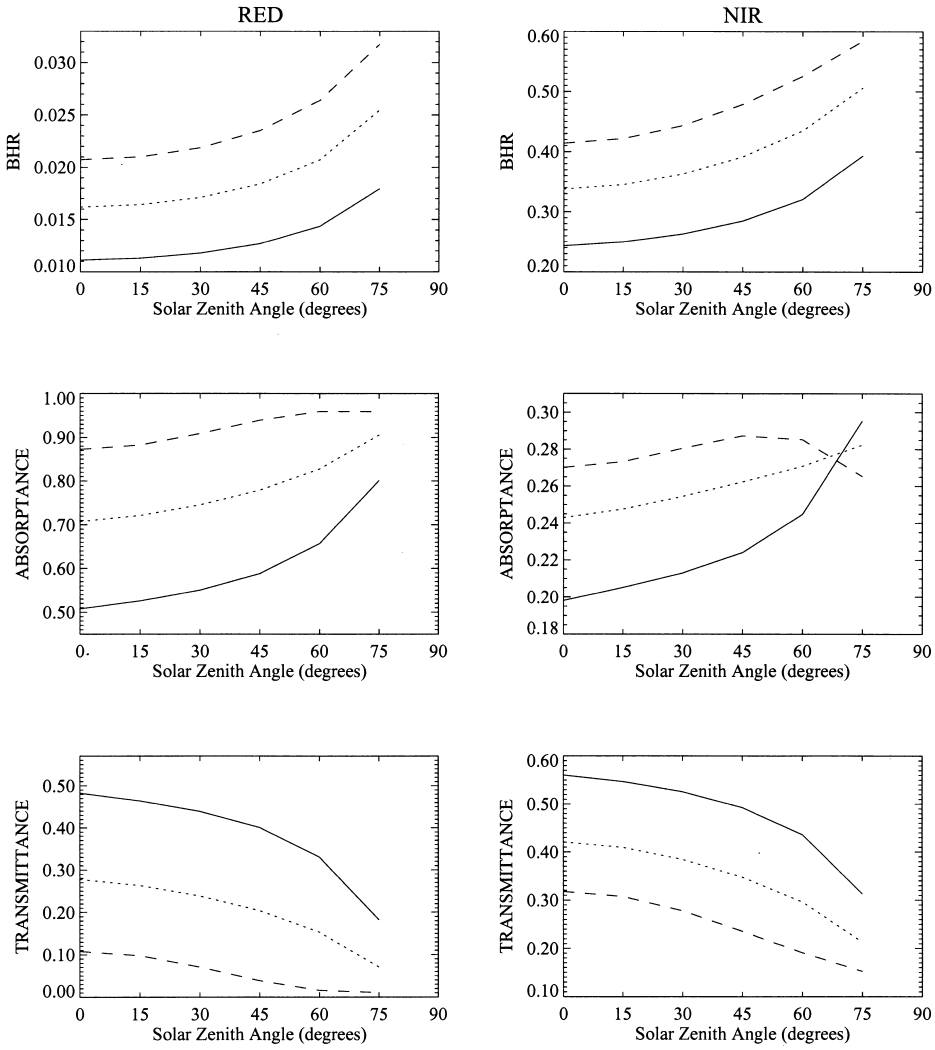


*Figure 10.* Influence of clumping on radiation regime in vegetation canopy at red (left) and near-infrared (right) wavelengths. BHR, absorptance, and transmittance as a function of solar zenith angle evaluated at three values of groundcover, representing, varying degree of clumping: $p=1.0$ (dashed line), $p=0.75$ (dotted line), $p=0.5$ (solid line). In all cases LAI=5.

well as the classical stochastic equation, does not describe this phenomenon if we look for solution in class $C^2$ (standard continuously differentiable functions). Hence, we used an approximating classical formula for the hot spot. Further improvement in model performance can be achieved by more accurate modeling of geometrical shapes of vegetation canopy, utilizing a non-Lambertian model of soil.

*This research was made possible through grants NA 76GP0481 and NAS 5-96061; we gratefully acknowledge this support. The authors thank Dr. Privette, Dr. Holben and the AERONET team (especially Dr. Abuhassan) and Dr. Qin for providing the CIMEL field data from the Jornada PROVE campaign.*

## REFERENCES

Baghdadi, N., and Baret, F. (1998), Amelioration du modele de transfert radiatif SAIL a partur d'un modele de lancer de rayons: Cas du mais. *Rapport D'Active*, IRNA, Avignon (in French).

Bass, L. P., Voloschenko, A. M., and Germogenova, T. A. (1986), *Methods of Discrete Ordinates in Radiation Transport Problems*, Institute of Applied Mathematics, Moscow, pp. 21–23 (in Russian).

Borel, C. C., Gerstl, S. A. W., and Powers, B. J. (1991), The radiosity method in optical remote sensing of structured 3-D surfaces. *Remote Sens. Environ.* 36:13–44.

España, M., Baret, F., Chelle, M., Aries, F., and Andrieu, B. (in press), A dynamic model of maize 3D architecture: Application to the parameterisation of the clumpiness of the canopy. *Agronomie*.

Knyazikhin, Y., Kranigk, J., Myneni, R. B., Panferov, O., and Gravenhorst, G. (1998a), Influence of small-scale structure on radiative transfer and photosynthesis in vegetation cover. *J. Geophys. Res.* 103(D6):6133–6145.

Knyazikhin, Y., Martonchik, J. V., Diner, D. J., Myneni, R. B., Verstraete, M., Pinty, B., and Gobron, N. (1998b), Estimation of vegetation canopy leaf area index and fraction of absorbed photosynthetically active radiation from atmosphere-corrected MISR data. *J. Geophys. Res.* 103(D24):32239–32257.

Knyazikhin, Y., Martonchik, J. V., Myneni, R. B., Diner, D. J., and Running, S. W. (1998c), Synergistic algorithm for esti-

mating vegetation canopy leaf area index and fraction of absorbed photosynthetically active radiation from MODIS and MISR data. *J. Geophys. Res.* 103(D24):32257–32277.

Li, X., and Strahler, A. H. (1992), Geometric-optical bidirectional reflectance modeling of discrete crown vegetation canopy: Effect of crown shape and mutual shadowing. *IIEEE Transact. Geosci. Remote Sens.* 30(2):276–292.

Li, X., Strahler, A. H., and Woodcock, C. E. (1995), A hybrid geometric optical-radiative transfer approach for modeling albedo and directional reflectance of discontinuous canopies. *IEEE Transact. Geosci. Remote Sens.* 33(2):466–480.

Marchuk, G. L., and Lebedew, V. L. (1971), *The Numerical Methods in Neutron Transport Theory*, Atomizdat Publ., Moscow (in Russian).

Marshak, A. (1989), Effect of the hot spot on the transport equation in plant canopies. *J. Quant. Spectrosc. Radiat. Transfer* 42:615–630.

Marshak, A., and Ross, J., (1991), In *Photon-Vegetation Interactions. Applications in Optical Remote Sensing and Plant Ecology* (R. B. Myneni, and J. Ross, Eds.), Springer-Verlag. Berlin-Heidelberg, pp. 441–468.

Menzhulin, G. V., and Anisimov, O. A. (1991), In *Photon-Vegetation Interactions. Applications in Optical Remote Sensing and Plant Ecology* (R. B. Myneni, and J. Ross, Eds.), Springer-Verlag, Berlin-Heidelberg, pp. 111–138.

Myneni, R. B., Asrar, G., and Kanemasu, E. T., (1987), Light scattering in plant canopies: The method of Successive Orders of Scattering Approximations [SOSA]. *Agric. For. Meteorol.* 39:1–12.

Myneni, R. B., Nemani, R. R, and Running, S. W. (1991), Estimation of global leaf area index and absorbed PAR using radiation transfer models. *IEEE Transact. Geosci. Remote Sens.* 35(6):1380–1393.

Nilson, T. (1977), *The Penetration of Solar Radiation into Plant Canopies*, Academy of Sciences of the ESSR, Institute of Astrophysics and Atmospheric Physics, Tartu.

Nilson, T. (1991), In *Photon-Vegetation Interactions. Applications in Optical Remote Sensing and Plant Ecology* (R. B. Myneni, and J. Ross, Eds.), Springer-Verlag, Berlin-Heidelberg, pp. 161–190.

Pomranning, G. C., and Su, B. (1995), A new higher order closure for stochastic transport equations. In *Proc. International Conference on Mathematics and Computations, Reactor Physics, and Environmental Analyses*, American Nuclear Society Topical Meeting, Portland, OR, pp. 637–545.

Privette, J. L., Abuhassan, N., Holben, B., and Asner, G. P. (1999), Field measurement, scaling and satellite validation of surface bidirectional reflectance. *Remote Sens. Environ.* Submitted.

Ross, J. (1975), *The Radiation Regime and Architecture of Plant Stands*, Gidrometeoizdat, Leningrad (in Russian).

Shultis, J. K., and Myneni, R. B. (1988), Radiative transfer in vegetation canopies with an isotropic scattering. *J. Quant. Spectrosc. Radiat. Transfer* 39:115–129.

Stewart, R. (1990). *Modeling Radiant Energy Transfer in Vegetation Canopies*, M. S. Thesis, Kansas State University, Manhattan, KS.

Titov, G. A. (1990), Statistical description of radiation transfer in clouds. *J. of Atm. Sciences* 47(1):24–38 (in Russian).

Vainikko, G. M. (1973a), The equation of mean radiance in broken cloudiness. *Trudy MGK SSSR, Meteorological Investigations* 21:28–37 (in Russian).

Vainikko, G. M. (1973b), Transfer approach to the mean intensity of radiation in noncontinuous clouds. *Trudy MGK SSSR, Meteorological Investigations* 21:38–57 (in Russian).

Vladimirov, V. S. (1963), *Mathematical Problems in the One-Velocity Theory of Particle Transport*, Tech. Rep. AECL-1661, At. Energy of Can. Ltd., Chalk River, Ontario.

Zuev, V. E., and Titov, G. A. (1996), *Atmospheric Optics and Climate*, The series "Contemporary Problems of Atmospheric Optics," Vol. 9, Spector, Institute of Atm. Optics RAS (in Russian).